Università
Ca'Foscari
Venezia

Master's Degree programme – Second Cycle (*D.M. 270/2004*)
in Sciences and Technologies of Bio- and Nano-Materials (classe LM-53 - Material engineering)

Ca' Foscari
Dorsoduro 3246
30123 Venezia

Final Thesis

Raman spectroscopic analysis of zirconia toughened alumina ceramic (ZTA) in presence of different metal stains and ZTA retrieval femoral heads.

Supervisor
Ch. Prof. Pietro Riello
Ch. Prof. Giuseppe Pezzotti

Graduand
Matteo Zanocco
Matriculation Number 828115

Academic Year
2015 / 2016

"Un vincitore è solo un sognatore che non si è arreso"

"A winner is only a dreamer who did not give up"

Nelson Mandela

Abstract

Zirconia-toughened-alumina (ZTA) composites represent the latest trends in load-bearing materials for arthroplastic applications. Their improved fracture resistance as compared to monolithic ceramics is the result of a trade-off at the microscopic scale between crack-shielding effects (toughening) and load-bearing surface metastability (environmental degradation). Both effects arise from a peculiar polymorphic (tetragonal-to-monoclinic; T-M) transformation occurring in the zirconia particles dispersed in the alumina matrix of the ZTA structure. In an attempt to explain the phenomenological findings of this tranformation, an implemented analytical model for the kinetics of polymorphic transformation in ZTA composites for hip joints is proposed and discussed. The proposed model builds upon the so-called Mehl-Avrami-Johnson (MAJ) description of transformation kinetics, thus combining two overlapping processes: nucleation of monoclinic sites and their successive growth. However, the proposed implementations aim at introducing in the model the fundamental dependencies of two additional factors, namely the initial fraction of monoclinic polymorph (i.e., in the as-received state after manufacturing) and the presence of different types of metal stain (Ti, CoCr and Fe) on the ZTA surface. Clear hints for the non-negligible role of the above two factors on the overall environmental stability of the implant components were contained in the phenomenological analysis. In the treatment here, nucleation and growth steps at monoclinic sites are yet considered as the constituent of the overall transformation process, but the effective activation energy, Q, is considered as function of time and temperature through the growth exponent, n. In addition, we incorporated the effect of metal ions into the process of surface degradation according to a general analytical description of transformation kinetics for isothermal or isochronal evolutions. The kinetic parameters remain time and temperature dependent, and the model yet obeys the MAJ description for constant initial fractions. The analytical model, which has experimentally been verified according to *in vitro* experiments, appears to, at least partly, reconciling *in vitro* and *in vivo* data of ZTA transformation.

Contents

Chapter 1

Introduction

The hip, the second largest structure of the human body, with its primary role in locomotion, is exposed to a high number of risks, traumatic or not, that may lead to the condition known as osteoarthritis. Regardless of initial disease, the result is almost always the same: a condition characterized by pain, limitation of movements and compromised locomotor function.

Osteoarthritis also known as degenerative arthritis, degenerative joint disease, or osteoarthrosis, is a type of joint disease that results from breakdown of joint cartilage and underlying bone. The most common symptoms are joint pain and stiffness. Initially, symptoms may occur only following exercise, but over time may become constant. Other symptoms may include joint swelling, decreased motion range and, when the back is affected by weakness, numbness of the arms and legs.

The most commonly involved joints are those near the ends of the fingers, at the base of the thumb, neck, lower back, knees, and hips. Joints on one side of the body are often more affected than the other. Usually the problems come on over years. It can affect work and normal daily activities. Causes include previous joint injury, abnormal joint or limb development, and inherited factors. Risk is greater in those who are overweight, have one leg of a different length, and have jobs that result in high levels of joint stress. Osteoarthritis is believed to be caused by mechanical stress on the joint and low grade inflammatory processes. It develops as cartilage is lost with eventually the underlying bone becoming affected. As pain may make it difficult to exercise, muscle loss may occur. Unlike in rheumatoid arthritis, which is primarily an inflammatory condition, typically the joints don't become hot or red. Treatment includes exercise, efforts to decrease joint stress and pain medications. Efforts to decrease joint stress include resting or the use of a crutch. Weight loss may help in those who are overweight. Pain medications may include paracetamol (acetaminophen). If this doesn't work, NSAIDs such as naproxen, may be used but these medications are associated with greater side effects. Opioids if used, are generally only recommended short term due to the risk of addiction. If pain interferes with normal life despite other treatments, joint replacement surgery may help. An artificial joint, however, only lasts a limited amount of time. Outcomes for most people with osteoarthritis are good.

In the past they have been designed and developed various surgical procedures including osteotomies, mergers and resections, without satisfactory results. Thus it emerged gradually the idea of joint replacement hip, also called arthroplasty.
Fifty years have now passed since the creation of the first modern total hip arthroplasty, by Charnley. Despite considerable efforts in improving the prosthetic design, especially for hip surgery, the Charnley's prosthesis, introduced in 1967, remans the gold standard. This is demonstrated by the fact that in joint replacement no other solution has generated a similar "revolution".
In its current form, the total hip replacement (*total hip arthroplasty*, THA) is one of most successful operations in modern orthopedic surgery because it allows patients, suffering from debilitating diseases, to improve the quality of life by restoring the joint function and removing pain.
Some information about operation of hip replacement in Italy, is available on the Istisan report 12/32 *"Progetto registro italiano ArtroProtesi (Riap): risultati della fase pilota sugli interventi di protesi d'anca"*: it is about 60,000 interventions, carried out in 220 facilities. Further study about operation of hip replacement, is available in the article *"Il Registro italiano ArtroProtesi (Riap): stato dell'arte"*, that is in Italy in 2010 there was 90000 hip replacement surgery. Among them, most are interventions primary total hip replacement (59631), followed by the partial (23916) and the revision surgeries (7342).
The hip replacement surgery allows patients suffering from disabling diseases (femoral neck fracture, osteoarthritis and dysplasia of the hip) recovery of a high quality of life with a life of the prosthesis, in 90 % of cases, more than 10 years. This procedure allows to solve or alleviate the painful symptoms and significantly improve physical and motor abilities of the patient.

1.1 Anatomy of the hip

The hip joint is one of the most important joints in the human body. It allows us to walk, run, and jump. It bears our body's weight and the force of the strong muscles of the hip and leg. Yet the hip joint is also one of our most flexible joints and allows a greater range of motion than all other joints in the body except for the shoulder.
The hip joint is a ball-and-socket synovial joint formed between the coxal (hip bone) and the femur. Cup-shaped structure on the coxal bone, known as the acetabulum, forms the socket for the hip joint. The rounded head of the femur forms the ball of the joint.
Hyaline cartilage lines both the acetabulum and the head of the femur, providing a smooth surface for the moving bones to glide past each other. Hyaline cartilage also acts as a flexible shock absorber to prevent the collision of the bones during movement. Between the layers of hyaline cartilage, synovial membranes secrete watery synovial fluid to lubricate the joint capsule. Around the hip joint there are many tough ligaments that prevent dislocation.
The strong muscles of the hip region, also help to hold the hip joint together and prevent

dislocation. Functionally, the hip joint have a very high range of motion. The ball-and-socket structure of the joint allows the femur to circumduct freely through a 360° circle. The femur may also rotate around its axis about 90° at the hip joint. Only the shoulder joint provides as high of a level of mobility as the hip joint. In addition to being flexible, each hip joint must be capable of supporting half of the body's weight along with any other forces acting upon the body. During running and jumping, for example, the force of the body's movements multiplies the force on the hip joint to many times the force exerted by the body's weight. The hip joint must be able to accommodate these extreme forces repeatedly during intense physical activities.

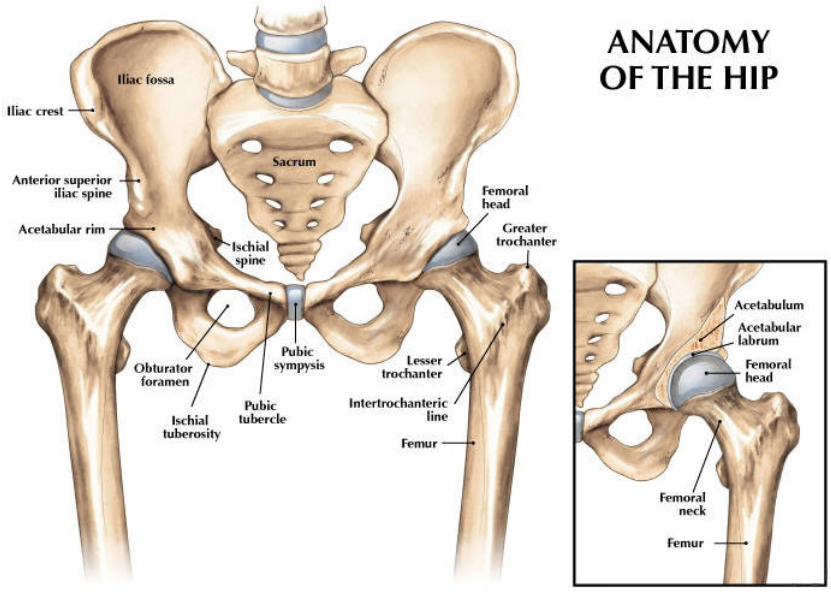

Figure 1.1: Anatomy of the hip.

The femur, or thigh bone, is the longest, heaviest, and strongest bone in the human body. All of the body's weight is supported by the femurs during many activities, such as running, jumping, walking, and standing. Extreme forces also act upon the femur thanks to the strength of the muscles of the hip and thigh that act on the femur to move the leg. The femur is classified structurally as a long bone and is a major component of the appendicular skeleton.

On its proximal end, the femur forms a smooth, spherical process known as the head of the femur. The head of the femur forms the ball-and-socket hip joint with the cup-shaped acetabulum of the coxal (hip) bone. The acetabulum is a cup-like depression ball and socket joint. The ilium, the ischium, and the pubis bones form it. The rounded shape of the head allows the femur to move in almost any direction at the hip, including circumduction as well as rotation around its axis. Just distal from the head, the femur narrows considerably to form the neck of the femur. The neck of the femur extends laterally and distally from the head to provide extra room for the leg to move at the hip joint, but the thinness of the neck provides a region that is susceptible to fractures [1].

1.2 Causes that lead to the operation

The most common condition for which you are running the total hip arthroplasty is a serious osteoarthritis, responsible for 70% of cases. The primary indication that leads to intervention is the severe pain, which also causes a restriction in daily activities. The main cause of pain, is represented by the deterioration of the cartilage, the function of which is precisely to make sliding the articular surfaces. Different causes, other diseases such as osteoarthritis, which lead to the total hip replacement can be:

- Post-traumatic osteoarthritis: This can follow a serious hip injury as a fracture or dislocation. Fractures of the hip bones that have suffered trauma over time can damage the articular cartilage, causing pain and limiting its function.
- Avascular necrosis: A hip injury, such as a dislocation or a fracture also, in some cases, can restrict the blood supply to the femoral head that ends up losing vitality in some of its parts or completely. The lack of blood can cause the collapse of the dead bone surface, which will result in osteoarthritis.

Most of the patients, after the operation, obtains an improvement of motor functions, but the main goal is the reduction of pain. Generally it's preferred the total arthroplasty in less active patients and over 60 years for at this age children are the performances required to the prosthesis and, in addition, the longevity intervention approaches to the expectation of the patient's life. With regard to the average life of an artificial joint prosthesis, this is about 8-12 years although, unfortunately, the duration is reduced for younger and active people. Despite the high level of success, total hip replacement from time to time is associated with complications (see Section 1.4).

1.3 Total Hip Arthoplasty (THA)

The hip replacement is an artificial joint made of metal alloys, plastic and/or ceramics materials, which replaces both the ill and altered parts of the joint. Eliminating the source of the pain in an effective and permanent allows the patient to an improvement in joint mobility. The hip prosthesis generally consists of two components: the acetabular cup, fixed the iliac wing of the basin, and the femoral component, inserted into the medullary canal of the femur. The cup, generally metal, in which is positioned an insert of polyethylene or ceramic liner , and the metal stem on the upper end of which, called the neck, it is inserted a metallic or ceramic head. The stem and the cup can be firmly fixed to the bone using polymethylmethacrylate cement (cemented prosthesis) or, as is increasingly the case, simply inserting the prosthetic components in the seat properly prepared, without the use of cement (non-cemented prosthesis). These latter are generally made of titanium and have a porous surface and a coating (usually hydroxyapatite HA) for promote the growth of bone tissue

around the implant, thus giving rise to a biological fixing.
In addition to the classification according to the method of attachment, any replacements prosthetic hip can be divided into three types according to the part of bone removed and replaced:

- The complete replacement, which provides for intervene on both articular components, the femoral head and acetabular
- Partial replacement, that does not change the acetabular;
- Partial prosthesis which provides for the retention of the neck of the femur (only young patients and in the absence of osteoporosis).

The hip prothesis it's made up of various components:

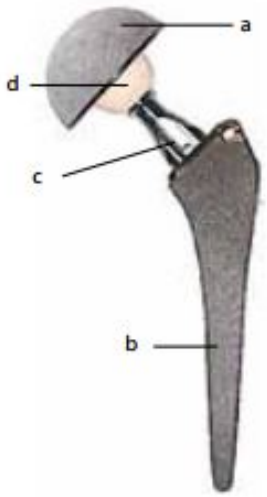

- The cup (or acetabular cup or acetabular prosthesis)(a): is the part that is attached to the pelvis by screws, surgical cement, screwing or mechanical forcing. It can present coated hydroxyapatite, which increases the biological anchoring, threaded or porous. The acetabular cup, generally metallic, in which it is positioned the acetabular liner that may be metallic, ceramic or plastic (Ultra-High-Molecular-Weight-Polyethylene UHMWPE);
- The metallic stem (b): is the part that is inserted into the femoral cavity and is fixed by cement surgical or mechanically. It also may be coated by a layer of hydroxyapatite to increase osteointegration;
- The neck (c): It can be defined as the stem portion that joins the head, or the clip ring, to the body of the stem;
- The femoral head (d): it is the terminal part of the femoral component, which mates with the internal cavity of the cup to form the artificial hip. The head can be a single piece with the stem or modular, that is separated from the femoral stem and attached to it during the intervention means of conical coupling. The materials used for the femoral head are metallic or ceramic.

The materials used for the construction of the hip prosthesis must meet several requirements:

- high strength and good stiffness properties, to ensure that stress is kept within acceptable limits and that there is a good geometric stability that permitting the proper functioning of the prosthesis;
- high mechanical strength;
- high chemical and wear resistance;
- good biocompatibility.

Today most of the hip prosthesis consists of an acetabular cup of Ultra-High-Molecular-Weight-Polyethylene (UHMWPE) or ceramic, a femoral stem made with metal alloy (in particular stainless steel, alloys of cobalt-chromium or titanium), and a femoral head made of metal (cobalt-chromium or titanium) or ceramic (usually Zirconia-Toughened-Alumina ZTA).

1.4 Causes of hip replacements

The hip replacement can have multiple causes [2]. Now we explain the most important.

- FRACTURE.

  The incidence of fracture, which is now about 1%. A higher incidence of fractures (6%) occurs instead in the revision arthroplasties with prostheses. The femur is the most common point of fracture, both during the primary procedure and during the revision, while the acetabulum fractures and pubic ramus captain only rarely. The fracture can occur in the bone, is urged by a trauma, is due to a severe osteolysis around the implant, due to wear. One speaks in this case of pathologic fracture that occurs only for bone weakness, even without a violent trauma or a fall.

- DISLOCATION.

  The leaking of the femoral head from the acetabulum cavity occurs with a percentage ranging from 1% to 3% in patients undergoing primary surgery. The main causes of displacement include poor adherence of the patient to the post-operative precautions and malposition of the prosthetic components, especially the acetabulum, during the operation. Dislocation and loosening, is one of the most important causes of revision. Most of the dislocations occurs within six months after surgery and almost all patients can be managed conservatively, if dislocations are occasional. Instead recurrent dislocations, which may cause the instability of the system or wear of the acetabular component, requiring surgical revision and then the replacement.

- COMPLICATION OF WOUNDS.

  Total hip arthroplasty complications of injuries that are most worthy of note are: the hematoma, with a total incidence of 3.5%, and infection that can occur as a secondary complication. The hematoma can, in fact, act as a breeding ground for bacteria. Some

local skin alterations that can disturb the wound healing are: the flare, hypertrophy, necrosis and septic complications. However infections superficial wound are rare and must be differentiated from the deep infections involving the prosthetic component.

- INFECTION (SEPTIC MOBILIZATION).

  The bacterial load on the prosthesis before implantation can be easily eliminated by treating the contaminated surfaces with disinfectants, or prevented using implants and sterile surgical procedures. The bacterial growth on the prosthesis after implantation instead is a critical issue; is in fact also a small enough number of microorganisms to contaminate the implant. The bacteria, given their great ability to adhere to the tissues and to the installations, they form complex multi-layer structures on the surface of the prosthesis, called biofilm, which act as true chemical-physical barriers capable of protecting the bacteria from the attack of antibiotics and the immune system. One of the most common contaminants is *Staphylococcus epidermidis* a skin bacteria that turns out to be very harmful if unable to enter the body. Bacterial contamination is therefore the most common cause of both acute infections of both chronic ones. The formation of bacterial biofilms can also be the cause of fatal infections which require the removal of the prosthesis [3].

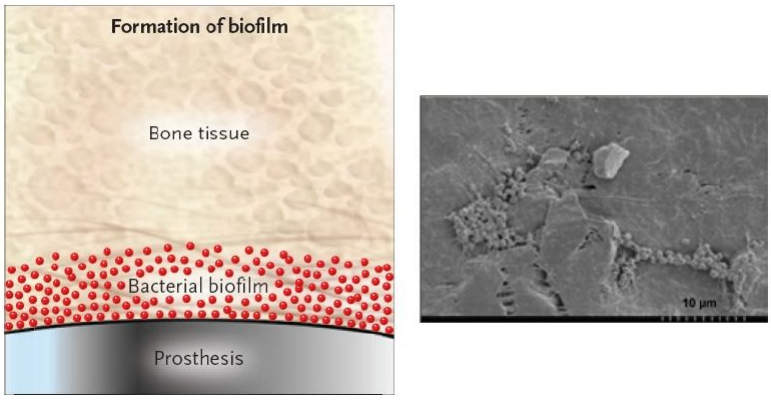

Figure 1.2: Bacterial biofilm on the prothesis.

Most studies report a lower rate of infection than 1% arthroplasty total primary and revision arthroplasty in this rate is more than 3%. Infections diagnosed within the first weeks after surgery or during the year, next they are mostly due to contamination during the operation.

- WEAR.

  Being a mechanical joint, the prosthesis undergoes wear with the formation of bone debris. The normal use of a joint prosthesis involves the cyclical articulation of head in the acetabulum. The considerable contact forces, localized at the interface between the metal or ceramic ball and the cavity corresponding covered in polymeric material, scratch the polymer causing the detachment of fibrils from the surface. These, in their turn, are crushed, giving rise to the formation of microscopic particles that generate

an inflammation that, with the passage of time, chronic, or may in some cases, degenerate. The lost material, released near the implant, triggers the body's reaction that called macrophages, cells which try to engulf the microfibrils of polymeric material. Macrophages engulf the particles to try to digest it but, given the presence of a significant amount of indigestible foreign material, fail to combat them all. This macrophages become enlarged and blend with other thus giving rise to giant cells, also called Langhans's cells or foreign body cells. These create, in turn, chronic inflammation and granulomatous process leading to the mobilization of the prosthesis, also macrophages, stimulated by the presence of debris, produce cytokines. These protein, secreted in response to a given stimulus, are capable of change the behavior of other cells by inducing new growth activities, differentiation or, as in the case considered, death. Cytokines fact stimulate both osteoclast activity, that "eat" the bone, which produce fibrous tissue. The final result is then the loss of bone tissue.
The forces acting in mutual sliding between materials can, in addition to the polymer erode, causing a geometric deformation ruin to the point that there is no more perfect coupling and alignment between the components. This cause a bad patient ambulation. The wear, which is closely linked to erosion, and then causes two effects in the body, one of pathological kind or chronic inflammation and one of the clinical type, that is a bad ambulation. Worn dentures must be removed and replaced with a new facility. The removal operations involve, inevitably, the ablation of a certain amount of bone and the substitution therefore, generally, can be implemented only once.

- ASEPTIC MOBILISATION OR LOOSE IMPLANT.
  The aseptic loosening of prothesis, so named because it was not associated with infectious phenomena (occurs i.e., in the absence of bacteria), is the expression of an insufficient stability of the prosthesis which involves, precisely, a mobility of the same with bone pain and resorption. The loss of fixation of the prosthetic component to bone is characterized by a periprosthetic radiographically detectable bone resorption, even before the patient feels pain. The global aseptic loosening (i.e., the cup and stem), continues to be a major cause of failure of the hip replacement and is more present in younger subjects and increased body mass. It is the most frequent long-term complications accounting for 80% of cases and is the most frequent reason for revision.
  Failure to secure the stem is evident radiographically almost always within one year intervention and is determined by a looseness to it happening. The easing of the cavity, mainly due to wear, represents a much more complex problem and because its changes are three-dimensional and it is not so easy to study them in a single x-ray (a contrast x-ray may be handy, though it is not justified in everyday use), and because this problem does not occur until after the seventh year.
  Whatever the mechanism that leads to the mobilization, this is certainly favored by the lack of stability of the implant in the immediate post-operative. Immediately after surgery you may notice a soft tissue layer at the interface bone-implant, with poor

mechanical properties, which can be composed of:

- Blood clots generated by the normal healing process;
- Bones scraps that have not been entirely removed prior to insertion of the stem;
- Organic fluid.

In this phase, the tissue surrounding the prosthesis is subject to an intense biological adaptation activities. In the majority of cases this adaptive process leads to the complete integration of the implant surface with the bone tissue. The regions with the soft tissue are sporadic and limited, while the interface can show the presence of bone bridges which guarantee the stability of the implant in any physiological condition of load. This process is called osseointegration, and is the source of secondary stability. However, the excessive amount of soft tissue, if it is not reabsorbed or osteointegrated, could trigger a degenerative process that self-sustaining, leads at first to the mobilization and then to the final prosthetic failure. This phenomenon is the primary cause of aseptic loosening.

A second cause is due to mechanical factors, such as the presence of micro-movements, due to the different characteristics of the materials in contact (e.g., the different stiffness of the structures) that can cause the production of debris, metallic or polymeric [4]. In 1975 Charley noticed first the presence of osteolytic processes but attributed the problem to infection. In 1976 Harris signaled instead of four cases of extended bone resorption, with mobilization of cemented stems, in the absence of infection. It thus identified the "cement disease" also called hereinafter, "from debris disease". Initially it was thought that the cause of this disease was due exclusively to the use of cement. A study on the incidence aseptic slackening in the first-generation cementing techniques revealed a high mobilization rate, while more recent studies, carried out on the second-generation cementing techniques, showed a reduced rate easing. The beginning of the failure of a cemented prosthesis is cement-prosthesis interface. For this reason, in the 70s, it concentrated on the construction of new models uncemented. Were Brown and Ring, in 1985 to indicate the presence of osteolytic areas even in non-cemented prosthesis. It is therefore understood that the aseptic loosening is the result of a new disease: the disease from debris. It is a biological reaction to particulate matter generated by wear of the prosthetic components [5].

The wear it produces the delamination of the polymeric material, with formation of billions of tiny polymer particles that spread in the surrounding synovial fluid. The immune system tries unsuccessfully to digest freeing degradative enzymes that, with time, can cause cell death of the adjacent bone tissue. The presence of particles, caused by wear between the stem and the cavity, and then triggers a cellular process that cause osteolysis. The progressive osteolysis is the cause of the mechanical system mobilization that eventually must be replaced. The severity of the disease from debris and the speed in the cause implant loosening, through the periprosthetic bone resorption, are determined by a number of factors such as:

- amount, size and type of debris;
- access of debris at the bone-implant and bone periprosthetic;
- organic response to debris, which varies from individual to individual.

With the wear word is then defined as the consumption of the prosthetic components that form the joint coupling between the head and the acetabular insert. In particular, the coupling which involves the use of polyethylene (plastic material used to reduce friction) has the highest incidence of wear, compared to the other pairs (ceramic-on-ceramic or metal-on-metal). The order of the substances, on the basis of the formation of debris, is the following: polyethylene, polymethyl methacrylate, metal and ceramics. They are studying alternative materials, such as the 2nd and 3nd generation polyethylene, which minimize the risk of wear and the consequent production of debris, ensuring greater joint stability. They are also the systems study to pharmacologically modulate the biological reaction to debris and inhibit bone resorption around the implant.
A third cause, which can trigger the separation process plant and osteointegrated therefore lead to mechanical loosening of the prosthesis, it is the occurrence of voltages exceeding the mechanical strength of the interface. In this context, the occurrence of micro-movements of a certain level may lead to the formation of fibrous tissue, with consequent worsening of the mechanical characteristics of the interface. The fibrous tissue is a soft tissue, rich in collagen fibers and microscopically similar to connective tissue, but with a structure and with characteristics that resemble those of cartilage. The fibrous layer that is generated around the implant walls results in poor anchorage implant to the bone tissue. The fibrous tissue, in fact, is not able to stabilize the prosthesis which then is subject to micro-movements of ascending magnitude; these, in turn, stimulate the production of new fibrous tissue. The process just described it is defined as "aseptic loosening" and is a gradual process in which they are involved both mechanical factors (micro movements and tensions) and biological factors (training of fibrous tissue).
Finally, as other cause which can lead to bone resorption and the resulting prosthetic loosening, should be considered as stress shielding the bone surrounding the implant, due to a mismatch in the structural behavior. The mechanical loosening derives in fact from a load that exceeds the strength of the prosthetic material or its interface with the bone. The excessive load may be due to a user out of the ordinary, to a model prosthetic inappropriate or to a wrong insertion technique. The phenomenon of stress shielding, induced by the element prosthetic more rigid, causes a reduction in bone mass, trabecular and cortical bone, which in turn reduces bone strength and its ability to withstand the loads transmitted. The reduction in bone mass can reach values of 50% after a few years [4]. Other causes of minor importance which combine to determine the aseptic loosening is:

- the quality of bone where the implant is placed;

  - the mechanical and geometric changes related to the aging process, both for the lower capacity osteoporotic bone to offset the high stiffness of the plants, both for the increase of the internal dimensions of the medullary canal.

- BREAKING OF PROSTHETIC COMPONENTS.

  The breakage of a component of the prosthesis may occur in connection to a violent trauma or because of minor but repeated trauma. The parts of the implant that are most subject to breakage are the neck, the stem and, more rarely, the acetabular and the femoral head. In these cases, intervention only replace the prosthetic parts that have deteriorated.

Chapter 2

Ceramic materials

In this chapter we will explain the history and properties of different materials for biomedical use. The Figure 2.1 shows the timeline of the discovery and use of some of these materials.

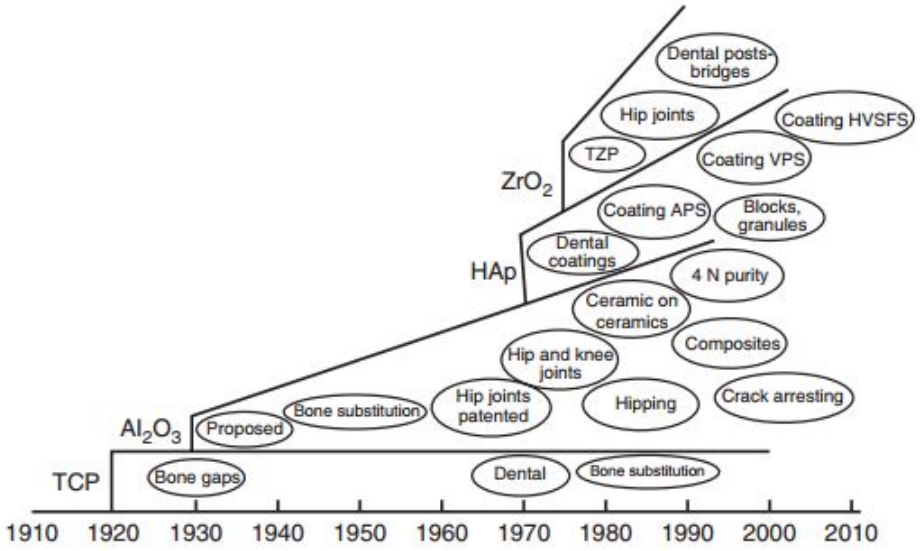

Figure 2.1: History of ceramics material for medical devices.

In the next sections, we will discuss in more detail some of the best materials still used in biomedical applications.

2.1 Alumina

Aluminum oxide (or alumina) is the aluminum ceramic oxide characterized by the chemical formula Al_2O_3. This material, apparently very brittle and of little use, is rather fundamental in the industrial field, for its properties such as resistance to acids, the high thermal conductivity, low electrical conductivity and is also a catalyst of industrial interest. It is used in many fields, such as the brick industry, refractory and ceramics materials, electronics and mechanics, as well as being used in biomedical as graft material.

The first uses alumina as a biomaterial can be found before the year 30. The first to con-

sider the possibility of using a ceramic material to replace a joint was Rock that presented a patent for the use of alumina ceramic [6]. Because of the relatively low strength, purity, and the experience developed before the war, the ceramic alumina needed another 30 years to develop, until Sandhaus in 1965 [7] proposed and patented an alumina for joints, called "*Degussit al 23*" and regarded as the "mother" of the technological ceramics today.

2.1.1 Properties

The alumina oxide used for biomedical applications is typically α-alumina, also known as corundum. In nature there are different single crystals with different impurities, such as Cr_2O_3 or Ti, that give a different color to alumina.

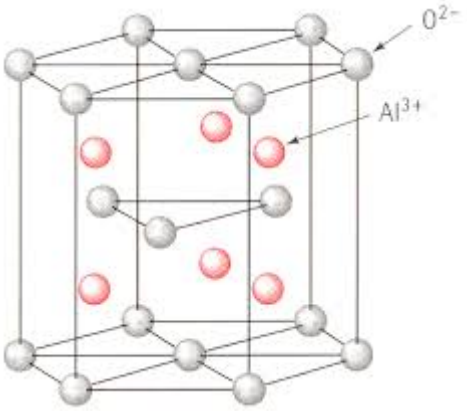

Figure 2.2: Crystallographic structure of α-alumina.

The molecule of aluminum oxide is characterized by a high ionic energy and a covalent bond that makes it one of the most stable oxides. This property makes it inert to galvanic reactions and makes it very stable chemically, even in very acidic or basic conditions at high temperatures. Alumina works very well in compression, but it is brittle under tension. Like most ceramics, alumina does not show (at ambient temperature) plastic deformation before fracture (e.g., no yield strength before fracture show in the stress-strain curve), and once started fractures progress very rapidly (low toughness).

In general terms, the resistance to traction of alumina improves with higher density and smaller particle size. Alumina producers carefully selected raw materials and the production process is strictly controlled to optimize the mechanical properties. With the introduction of low-melting MgO ceramic in the process, mass transport was improved during solid state sintering, and ceramics reached full density at lower temperatures. The effect is a strong decrease in grain growth, so an increase of the resistance of the ceramic. The reduction in hardness due to the introduction of MgO is compensated for by additions of small amounts of Chromia (Cr_2O_3).

Able to particular alumina medical attention is to reduce CaO ceramic content as they may affect the mechanical properties of alumina in a wet environment. Even the presence of NaOH impurities in the powders obtained by the Bayer process, makes them unsuitable for the hi-tech biomedical application. Continuous efforts to improve the properties of

bioceramics alumina have been made, e.g. by the introduction of high purity raw materials, hot isostatic pressing, to verify on 100% of the components product testing.
Hot isostatic pressing (HIP) is a manufacturing process, theorized in the 1970s, used to reduce the porosity of metals and increase the density of many ceramic materials. This improves the material's mechanical properties and workability. The HIP process undergo a component to elevated temperature and isostatic pressure. The pressurizing gas most widely used is argon. An inert gas is used, so that the material does not chemically react. The chamber is heated and increase the pressure inside it. Pressure is applied to the material from all directions (hence the term "isostatic")
A further improvement of the process is the introduction of components in the test trial. The test consists in the application of internal pressure to the spherical head (or to the inlay). This induces a stress close to the maximum capacity of the component load. When applied to 100% of manufactured parts, faulty products can be eliminated before the final inspection. Even the improvements in the traceability components due to the introduction of laser marking contributed to improving the overall quality of the manufacturing process [8].
During the early years of clinical use, some ball heads were soon withdrawn from the market because of unacceptable fracture rate [9]. Today the failure of alumina ball heads are typically associated with severe traumatic accidents, or technical errors. As a result of productivity improvements, fracture of alumina ball heads today very low frequency.

2.2 Zirconia

Zirconia, the metal oxide (ZrO_2), was identified as such in 1787 by the German chemist Martin Heinrich Klaproth, as the reaction product obtained after heating of some gems, and has been used for a long period mixed with rare earth oxides as pigment for ceramics [10]. Good chemical and dimensional stability, mechanical strength and hardness, coupled with a Young's modulus in the same order of magnitude of stainless steel alloys is the origin of the use of interest zirconia as a ceramic biomaterial [9]. As can be seen in the Figure 2.1 the development of zirconia as a material for biomedical application dates back to the mid-70s, even if the first publication of the application of zirconia as a biomaterial dates back to 1969 by Helmer and Driskell [11] while the first publication concerning the use of zirconia for construction of femoral heads for total hip replacements, one of the areas of greatest use, was introduced by Christel et al. [12] in 1988. The main use of the zirconia is in the production of ceramics [11] [12], but there are many more other uses including the protective coating on particles of titanium dioxide pigments, as a refractory thermal insulation material, such as abrasive and polish. The stabilized zirconia is used in the oxygen sensor and in fuel cell membranes, due to its ability to allow oxygen ions to move freely through the crystal structure at high temperatures. This high ionic conductivity (and a low electronic conductivity) makes it one of the most useful ellectro-ceramics [13]. The zirconium dioxide is also used as a solid electrolyte in electrochromic devices.

The high breaking strength shown by many of zirconia ceramics is attributed to the bonding that occurs in the transition from tetragonal to monoclinic phase and its output during the propagation of the fracture (which will explain in later section).
In other zirconia ceramics containing tetragonal phase, the high toughness is associated with the ferroelastics domain switching. However, many of these interesting characteristics of zirconia, especially the resistance to fracture and stiffness, are compromised after prolonged exposure to water vapor at intermediate temperatures ($\sim 30° \div 300°$ C) according to a process called low-temperature degradation (LTD), identified for the first time more than twenty years ago. This applies, in particular to the zirconium oxide in biomedical applications, such as hip prostheses and dental implants [13].

2.2.1 Properties

As mentioned previously, the most important properties of zirconia are the high chemical stability, mechanical strength, high hardness and Young's modulus comparable to metals which makes it an excellent material for biomedical applications. However, like all materials it has weaknesses that need to be considered.

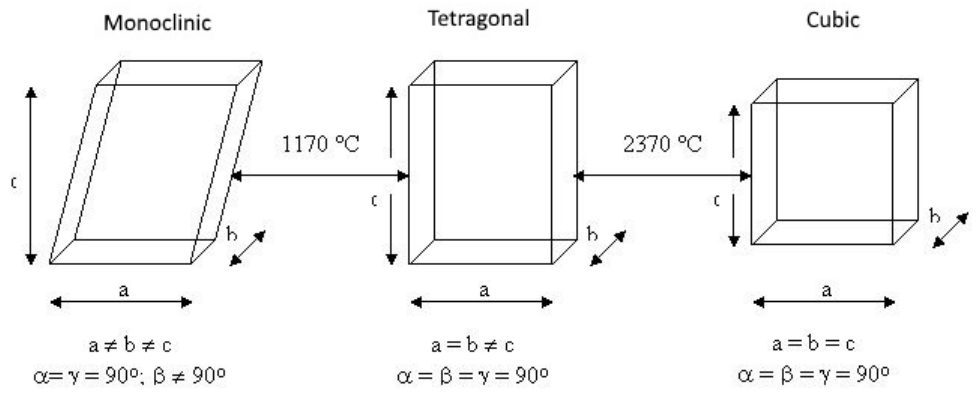

Figure 2.3: Allotropic forms of zirconia.

Zirconia has three allotropic forms: monoclinic (M), cubic (C) and tetragonal (T). Pure zirconia is monoclinic at room temperature. This phase is stable up to 1170°C. Above this temperature it is transformed into tetragonal and then in the cubic phase over 2370°C. During cooling, a tetragonal-to-monoclinic transformation (T-M) takes place in a temperature range of about 100°C under 1070°C. The phase transformation taking place, during cooling is associated with an expansion of about 3-4% volume [9] [14], stresses generated by the expansion gives rise to great stress which lead to the formation and propagation of cracks. To maintain the integrity of the oxide sintered zirconia at room temperature, one may or low-temperature sintering in order to maintain the monoclinic structure during sintering, which leads to a low resistance and toughness, or stabilize the tetragonal phase and the cubic phases at room temperature, thus avoiding the T-M transformation during cooling. The basic approach to the engineering of zirconia and avoid a transformation and formation

of cracks was described by Ruff and Ebert [15] almost a century ago remains valid today: pure zirconium alloy with another oxide to stabilize completely or partially tetragonal phase and/or the cubic phase.

The addition of stabilizing oxides, such as CaO, MgO, CeO, Y_2O_3 to pure zirconia, create different microstructures for different uses. They are generally divided into three broad categories according to their structure: FSZ, PSZ and TZP respectively fully stabilized zirconia, partially stabilized zirconia and tetragonal zirconia polycristals. In FSZ the zirconia is the cubic phase with the addition of 8% of Y_2O_3, normally used for oxygen sensors, and fuel cell electrolytes. The PSZ consists of nano particles of monoclinic or tetragonal zirconia dispersed in a matrix of cubic zirconia. The TZP is usually considered monoliths of tetragonal phase which is usually contained in a cubic phase. Usually the TZP stabilized with yttria or cerium [13]. These precipitates or may be in the grain boundaries or inside of the cubic array.

In 1972 Garvie et al. [16] showed an increase in mechanical strength of the PSZ was improved by a homogeneous and fine distribution of the monoclinic phase in the cubic matrix. The engineering of zirconia was marked by Garvie et al. [17] which shows how to make the most of the transformation of tetragonal to M-PSZ in increasing the mechanical strength and toughness of zirconia.

They observed that the metastable tetragonal precipitate, finely dispersed within the cubic matrix, were able to transform into monoclinic phase when the force exerted from the cubic matrix was missing, that is, with the advance of a crack in the material. In this case the stress zone associated with the phase transformation is in opposition with the stress caused by the advancement of the crack. You get a hardness increase because the energy associated with crack propagation is dissipated both in the T-M phase transformation both in increasing the volume of the latter.

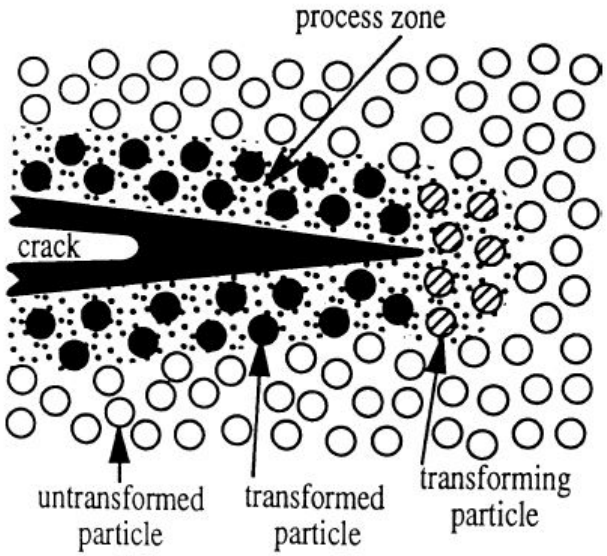

Figure 2.4: Crack propagation pattern.

The development of this metastable tetragonal precipitate is obtainable by an addition of 8 mol% of MgO to zirconia. PSZ can also be obtained by adding yttria to zirconia but you can also get the TZP formed only by zirconia in the tetragonal phase. TZP usually contains 2-3 mol% of yttria and is renamed Y-TZP and is completely made up of tetragonal phase with a grain size of around 100nm. The fraction of tetragonal phase maintained at room temperature depends on the size of the grains, the amount of stabilizer (yttria) and on stress exerted on the grain matrix. The mechanical properties of the TZP are highly dependent on these parameters.

It's very important to consider the nature of the metastable tetragonal grains. The critical grain size exists and is linked to the concentration of yttrium oxide, above which the spontaneous T-M transformation of the grains takes place, while it would be inhibited by too fine a distribution of the grain [18]. An interesting feature of the transformation toughened zirconia is the formation of stress on their surface [19]. Tetragonal grains on the surface are not bound by the matrix, and it can transform to monoclinic spontaneously, e.g. by abrasive processes that can induce compressive stresses to a depth of several microns below the surface. The phase transition on the surface and the subsequent surface hardening can have a significant role in improving the mechanical properties and wear parts of zirconia, the thickness of the transformed layer is one of the limit conditions. The T-M process of transformation on the surface may cause the origin of cracks on the surface, increase the roughness due to the increase of volume of the monoclinic grains followed by the expulsion of some debris from the surface of the material with catastrophic effects for the mechanical properties and the wear of implant.

The degradation of mechanical properties in the zirconia, known as aging, is due to the spontaneous transformation from the metastable tetragonal phase to the monoclinic phase. This behavior occurs in the temperature range between 200° and 300°C in the presence of water vapor [20] [21]. The main degradation steps were summarized by Swab [22] according to this scheme:

- The critical temperature is in the range between 200°÷ 300 ° C;
- The aging effect leads to a reduction of hardness, strength and density and an increase of monoclinic phase;
- The decrease in mechanical properties is due to T-M transformation, creating micro fractures on the surface;
- The T-M transformation start from the surface and proceeds toward the inside of the material;
- Reducing the size of the grains and/or increasing the concentration of the stabilizer, can bring reduce the phase transformation but at the expense of mechanical properties;
- The T-M transformation is increased in aqueous or water vapor environment.

2.2.2 Current applications of zirconia and impact of T-M transformation

BIOMEDICAL SYSTEMS.

Biomedical implants are used to ensure that people could return to normal function after trauma or diseases that degrade the joints. Ceramic implants are used due to their biocompatibility and chemical inertness lasting more than ten years *in vivo*, all mandatory requirements for a ceramic implant body to resist stress and to many cycles of use. In 1990 the zirconia was introduced into the orthopedic field to replace the alumina for its high hardness [23].

The first stabilizers used were the calcium oxides (CaO) and magnesium oxides (MgO), but thanks to the high strength at room temperature, 3Y-TZP (3 mol% Y_2O_3- TZP) soon became the best material for these applications. In addition, it's possible to create the spheres (femoral head) with the smaller diameter (22mm) and installations for knees, where the alumina could not be used for these purposes. The clinical results reported before 2000 were satisfactory, with very low failure rates reported for zirconia femoral heads. However, in 1997 the US Food and Drug Administration (FDA) reported that the standard steam sterilization procedure (134°C, 2 bar), led to surface roughening of temporal head implants. More importantly, in 2001, the FDA announced that the distribution companies were recalling zirconia femoral heads due to a number of fractures.

The origin of the failures was related to an accelerated LTD in zirconia prothesis, and these had a great impact in the orthopedic field, in particular the major suppliers of orthopedic implants stopped the production of this type of system, and some of them went to the production of other composite materials with especially alumina and zirconia. This episode highlighted the role of LTD in zirconia implants. Many clinical and retrieval implant analysis studies were carried out in the implants of zirconia. They have shown that even the zirconia implants treated in the best conditions could suffer from a certain degree of *in vivo* degradation. Based on the analysis of retrieval, the degree of degradation varied from roughening, the decrease of hardness (due to microcracking) to failure (the slow crack growth) [24].

Many clinical studies show a significant increase in wear rate of zirconia femoral heads. The increase of wear rate becomes apparent after many years and is connected to a large decrease of the transformation T-M on the surface by varying the surface roughness and the shape of the ball. This also leads to a release of debris in the environment that then through the synovial fluid are dispersed in a greater area. The body's response with this debris is catastrophic; macrophages identify these particles as "hostile" for the body and attack them. Then macrophages release of pro-inflammatory cytokines that stimulate osteoclasts to bone resorption, resulting in osteolysis and eventual loosening of the prosthesis and need to implant replacement. It is unclear whether today wear and aging are synergistic effects, although you can expect that.

DENTAL IMPLANTS.

In the late '90s, the success of zirconia orthopedic implants encouraging development for dental implants as "crowns" or "bridges." In contrast with the trend in orthopedic implants to change the material for the problems of zirconia, in the dental implants it has increased the development of 3Y-TZP. Also in dental implants the zirconia is subject to LTD even if the temperatures are less than those which undergoes an inside implant. The possibilities of breakage of a dental implant or a review are still high, although less critical of an orthopedic implant, and producers should take account of this.

OTHER USES.

A major application of YSZ is as an ionic electrolyte solid oxide fuel cells (SOFC) and sensors, such oxygen sensors. The zirconia is used in its cubic shape and high temperature to maximize the ionic conductivity. Zirconia is also used as TBC. The primary function of a TBC is to provide thermal protection to the metallic engine components in a thermal gradient that allows them to be used in the presence of hot gases. The majority of applications involves the protection of the gas turbine blades, vanes, combustors and both aerospace and power generation turbines, but are also used in the cylinders of diesel engines and other situations in which, at high temperature, is required the insulation.

2.2.3 Alternative zirconia-based materials

The idea was to dope the zirconia with a lanthanide or actinide. The zirconia stabilized with ceria has been studied much as the YSZ and it was noticed that reduces the LTD problem. As can be seen from the data of El Attaoui [25] during the synthesis the structure is completely tetragonal and during the cooling becomes metastable following the phase transformation temperature. It can also be noted that zirconia doped with cerium has a lot of resistance during the effect of LTD respect to YSZ, but the phase transformation temperature is the same, then you can think that the driving forces of the transformation is the same. Another difference lies in the absence of vacancy that occurs in zirconia doped with ceria, at least in the state Ce^{4+}.

Since the LTD phenomenon is associated by the spread of OH^- ions inside of the vacancy, you can interpret the strength of zirconia doped cerium to LTD due to the absence of these vacancy. This suggests that the CeZr is preferred for biomedical use, compared to 3Y-TZP. It is also notable that as with the YSZs, increasing the concentration of ceria makes the zirconia even more resistant to LTD. One point is still under study is the possible presence of Ce^{3+} instead of Ce^{4+}. To will improve the resistance to the effect LTD, the choice of the dopant still remains a subject of study. To increase resistance to LTD must make sure that the T-M transformation temperature is as low as possible. They have tried many different doping as scandium, erbium, tantalum, yttria, but it is noticed how the element which has a lower processing temperature is cerium.

However, a zirconia with a low T-M transformation has a low hardness and a low transfor-

mation by hardening. It is possible to dope the zirconia with more than one element, even if the phase diagrams are not known, one tries to use two doping with different charges so as to keep controlled the percentage of vacancy in the zirconia. For example they have studied pairs of doping as the Y-niobia-Zr [26] and Y-Zr-tantalia [27] that has a high fracture by hardening without stress induced by the transformation.

Another system to improve the properties of the zirconia is create composite systems. Orthopedic part unite the properties of zirconia and alumina, with those we see a considerable reduction of the LTD. These materials are divided according to the type of major phase present in the composite. A problem encountered in this type of material is the fact that zirconia will be under large tension stress on the part of the alumina, which increases the transformation of metastable zirconia decreasing the resistance to the effect LTD. The residual stresses that occur depend on the volume fraction in the composite material. It is very difficult to believe that small amounts of alumina added to the zirconia matrix can change the properties such as the increase of the elastic stiffness of the material and therefore increase the elastic energy of deformation associated with the transformation of particles. Even the size of the grains depends on the amount of alumina added, typically the addition of a small amount of alumina reduces the size of the grains [28]. Moreover, with the added of impurities such as silica, it makes the water diffusion inside the material is slowed down mainly along the grain boundaries. Although the activation energy for the degradation varies depending on the volume of alumina addition. This suggests that the driving forces are not changed for the transformation.

Rather, the curves move to longer times, depending on the amount of alumina added, because only on the surface in contact with moist environments are present more alumina grains that zirconia. If we use as a major step we obtain the alumina zirconia toughened alumina ZTA or that we will discuss in the next section.

2.3 Zirconia-Toughened-Alumina(ZTA)

In the second half of the '70s, it was developed new ceramic materials. The introduction of zirconia in different percentages in α-alumina matrix they obtain a class of ceramic with high hardness [29]. Historically, contrary to its name, zirconia has been added to increase the strength of alumina, by limiting the grain growth. Two distinct classes of late contributions can be considered. The first is simply topological: if the phase of zirconia is not continuous micro structural, then there is not a path for diffusion of moisture species in the ceramic and thus the degradation can not proceed beyond the surface and in depth in the material. The second contribution is related to the metastable tetragonal phase of zirconia discussed in the previous section. Even if zirconia grains in ZTA are likely to be in net tensile stress after processing as a result of thermal expansion mismatch, the transformation is hindered by the much stiffer alumina matrix. [13].

2.3.1 Properties

The mechanical properties of ZTA are a mix between the properties of alumina and zirconia Y-TZP. As previously mentioned the alumina matrix exerts a force on the metastable tetragonal zirconia grains stabilizing them at this stage. The hardness of this material is due to T-M transformation of zirconia grains due to the difference in elastic modulus between the matrix and the particles of alumina zirconia, cracks will tend to move in the all around of the oxide particles of rigid zirconia, inducing their stage of T-M dissipating transformation so the crack energy [30]. An additional dissipative effect is due to micro-cracking of the matrix due to the expansion of the dispersed particles. The high density of the matrix and the optimization of the microstructure of the zirconia particles, which should keep the maximum of the metastable phase and ensure the processing of the maximum volume are the parameters that ensure the performance of the best materials.

In applications such as load-bearing orthopedic joints, where hardness is of fundamental importance, ZTA have some drawbacks, as the introduction of zirconia in alumina matrix results in a decrease in the hardness of the ceramic [31]. The observation that alumina may be tempered by addition of filaments (eg SiC filaments) is well known: the concerns about the carcinogenicity of filaments, and adhesion limits of the filaments to the matrix decreased the interest in biomedical applications of these materials . But elongated grains (platelets) can be nucleated within the structure of a ZTA ceramic, thus acting as a mustache. This can be achieved by adding, for example, strontium oxide (SrO) in the ZTA, thus obtaining the formation of $SrAl_{12}O_{19}{}^{-}$ reaction platelets in solid form in situ during sintering.

In the presence of chromium (Cr_2O_3) oxide system introduced to save the hardness of the alumina and the addition of yttria (Y_2O_3) oxide to stabilize the transformation of zirconia, it leads to the formation of a material which has the hardness of the alumina , the hardening due to the transformation of the zirconia grains and all enhanced by the presence of these platelets of SrO [32]. The properties of this ceramic have been used to develop various types of femoral heads with different diameter or with different designs. Lately they are developing these ceramic for biological applications with different designs and different issues such as the knee and the ankle.

Chapter 3

Raman

3.1 Introduction

When light interacts with matter, the photons which make up the light may be absorbed, scattered or may not interact with material and may pass straight through it. The process of absorption, requires that the energy of the incident photon corresponds to the energy gap between the ground state of a molecule and the excited state. It is the basic process used in a wide range of spectroscopic techniques. In contrast, scattering can occur whether or not there is a suitable pair of energy levels to absorb the radiation, and the interaction between the light and the molecule which causes this requires a different approach.

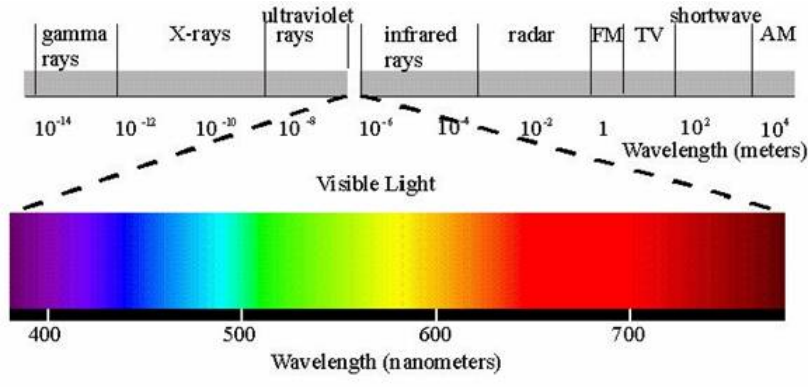

Figure 3.1: Light spectrum.

Radiation is often characterized by it's wavelength (λ), however, in spectroscopy, becouse we are inerested in the interaction of radiation with state of the molecule being examinated and this being usually discussed in terms of of energy, it's often useful to use frequency (ν) or wavenumber (ϖ) scale, which are linearly related wih energy.

$$\lambda = c/\nu \tag{3.1}$$

$$\nu = \Delta E/h \tag{3.2}$$

$$\varpi = \nu/c = 1/\lambda \tag{3.3}$$

The way in which the radiation interact with the materials between infrared and Raman spectroscopies is different. In infrared spectroscopy, infrared energy covering a range of frequencies is directed onto the samples. Absorption occurs where the frequency of the incident radiation matches that of a vibration so that the molecule is promoted to a vibrational excited state. The loss of this frequency of radiation from the beam after it passes through the samples is then detected.

Raman spectroscopy used a single frequency of radiation to irradiate the samples and it is the radiation scattered from the molecule, one vibrational unit of energy different from the incident beam, which is detected. Unlike IR absorption, Raman scattering does not require matching of the incident radiation to the energy difference between the ground and excitate state. In Raman scattering, the light interacts with the molecule and distort (polarizes) the cloud of electrons round the nuclei to form a short-lived state, called a "virtual state". This state is not stable and the photon is quickly re-radiated.

The energy changes we detect in vibrational spectroscopy are those required to cause nuclear motion. If only electron cloud distortion is involved in scattering, the photons will be scattered with very small frequency changes, as the electrons are comparatively light. This scattering process is regarded as elastic scattering and is the dominant process. For molecules it is called Rayleigh scattering. However, if nuclear motion is induced during the scattering process, energy will be transferred either from the incident photon to the molecule or from the molecule to the scattered photon. In these cases the process is inelastic and the energy of the scattered photon is different from that of the incident photon by one vibrational unit. This is Raman scattering.

It is inherently a weak process in that only one in every 10^6–10^8 photons which scatter is Raman scattered. In itself this does not make the process insensitive since with modern lasers and microscopes, very high power densities can be delivered to very small samples but it is does follow that other processes such as sample degradation and fluorescence can readily occur.

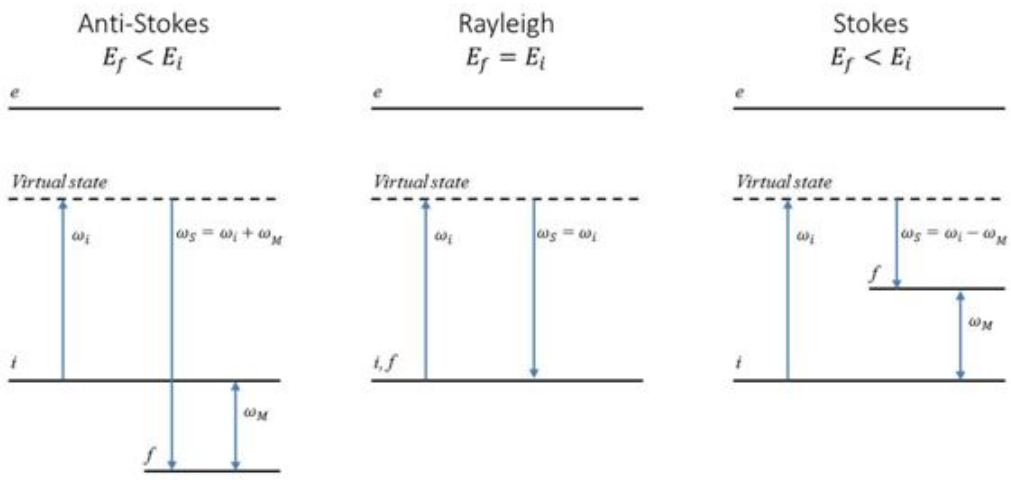

Figure 3.2: Energy level diagram for Anti-Stokes, Rayleigh and Stokes scattering process.

Figure 3.2 show the basic processes which occur for one vibration. At room temperature, most molecules, but not all, are present in the lowest energy vibrational level. Since the virtual state are not real states of molecule but are created when the laser interaction with the electrons and causes polarization, the energy of these state is determined by the frequency of the light source used. The Rayleigh process will be the most intense process since most photons scatter this way. It doesn't involve any energy change and consequently the light return to the same energy state.

The Raman scattering process from the grund vibrational state i leads to absorption of energy by the molecule and it's promotion to a higher energy excited vibrational state (f). This is called Stokes scattering.

However, due to thermal energy, some molecules may be present in an excited state such as i. Scattering from these state to the ground state f is called anti-Stokes scatteing and involves tranfert of energy to the scattered photon. The relative intensities of the two process depend on the population of the various states of the molecule.

3.2 Absorption and scattering

When a light wave, considered as a propagating oscillating dipole, passes over a molecole, it can interact and distort the electrons cloud arround the nuclei. This energy is released in the form of scattered radiation. In the visible region, the wavelength of the light is between 400 and 700nm whereas the size of a small molecule such as carbon tetrachloride is about 0.3-0.4nm. Thus the oscillating dipole is much larger than the molecule. If it interacts with the molecule as it passes, it causes the electrons to polarize and go to a higher energy state. At that instant, the energy present in the light wave is transferred into the molecule. This interaction can be considered as the formatin of a very short-lived "complex" between the light energy and the electrons in the molecule in which the nuclei don't have time to move appreciably.

This "complex" between the light and the molecule isn't stable and the light is released immediately as scattered radiation. It is often called the virtual state of the molecule. Since it has a different electronic geometry from that found in the static molecule and the nuclei don't have time to respond and reach a new equilibrium geometry to fit the distorted electronic arrangement, none of the electronic states of the molecule will describe the electron arrangement. Further the actual shape of the distorted electron arrangement will depend on how much energy is transferred to the molecule and hence is dependent on the frequency of the laser used. Thus, the laser defines the energy of the virtual state and the extent of the distortion. This virtual state is a real state of the transitory "complex" formed.

The process differs from an absorption process in a number of ways. Firsly, the additional energy doesn't promote an electron to any one excited state of the static molecule; all states of the static molecule are involved to different extents and are mixed together to form states of the distorted "complex". The energy of this state is depended on the energy of the laser used and the amount of distortion is dependent on the electronic propreties of the molecule

and on the energy of the laser.

Secondly, the lifetime of the excited state is very short compared to most absorption process. The radiation is scattered as a sphere and not lost by energy transfer within the molecule or emitted at a lower energy. Thirdly, there is a link between the polarization of the exciting and scattered photons which can be of value in assigning particular vibrations.

Two types of scattering are readily identified. The most intense form of scattering, Rayleigh scattering, occurs when the electron cloud relaxes without any nuclear movement. This is essentially an elastic process and there is no appreciable change in energy. Raman scattering on the other head is a much rarer event which involves only one in $10^6 - 10^8$ of the photons scattered. This occurs when the light and the electrons interact and the nuclei begin to move at the same time.

Since the nuclei are much heavier than the electrons, there is an apreciable change in energy of the molecule to either lower or higher energy depending on whether the process starts with a molecule in the ground state (Stokes scattering) or form a molecule in a vibrationally excited state (anti-Stokes scattering).

Figure 3.2 shows a simple diagra illustrating Rayleigh and Raman scattering. Most molecules at rest prior to interaction with the laser and at room temperature are likely to be in the ground vibrational state. Therefore the majority of Raman scattering will be Stokes Raman scattering. The ratio of the intensities of the Stokes and anti-Stokes scattering is dependent on the number of molecules in the ground and excited vibrational levels. This can be calculated from the Bolzmann equation:

$$\frac{N_n}{N_m} = \frac{g_n}{g_m} exp\left[\frac{-(E_n - E_m)}{kT}\right] \tag{3.4}$$

N_n is the number of molecules in the excited vibrational energy level (n);

N_m is the number of molecules in the ground vibrational energy level (m);

g is the degeneracy of the levels n and m;

$E_n - E_m$ is the difference in energy between the vibrational energy level;

k is Boltzmann's costant ($1.3807x10^{-23}JK^{-1}$)

We shall see, when we consider symmetry later in this chapter, that some vibrations can occur in more than one way and the energies of the different ways are the same, so that the individual components cannot be separately identified. The number of these components is called the degeneracy and is given the symbol g in Equation (3.4). Since the Boltzmann distribution has to take into account all possible vibrational states, we have to correct for this. For most states g will equal 1 but for degenerate vibrations it can equal 2 or 3.

3.3 States of a system and Hookes's law

Any molecule consists of a series of electronic states each of which contains a large number of vibrational and rotational states. In Figure 3.3 a sketch of a typical ground electronic state of a molecule is shown. The y-axis represents the energy of the system and the x-axis the internuclear separation. The curved line represents the electronic state.

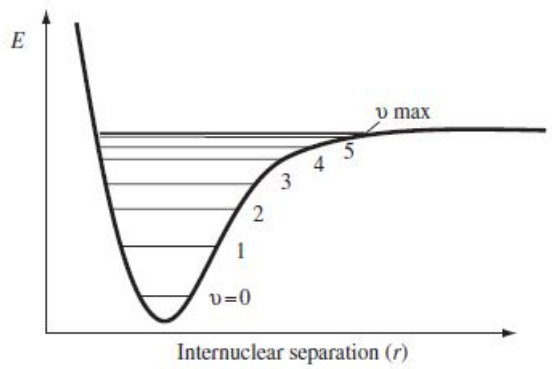

Figure 3.3: Tipical Morse curve for an electronic state showing the vibrational levels as horizontal tie lines.

At large internuclear separations, the atoms are essentially free and as the distance decreases they are attracted to each other to form a bond. If they approach too closely, the nuclear force cause repulsion and the energy of the molecule rises steeply as shown. Thus the lowest energy is at the bond length.
However within the curve, not every energy is possible since the molecules will be vibrating and the vibrational energies, which are quantized, have to be taken into account. The tie lines are the quantized vibrational states. A particular vibrational level of a particular electronic state is often called a vibronic level.
At first glance this curve, called Morse curve, is relatively simple but there are more complications which are generally not added becouse the diagram gets too cluttered for use. What is shown in the Figure 3.3 refers to one vibration.
The first level (v=0) is the ground state where the molecule is not vibrating and the second level (v=1) is the state where one quantum of the correct energy is absorbed and the molecule vibrates. The levels above this require energies of approximately but not exactly two times, three times, etc., of the quanta required to move the molecula from the ground state to the first excitate state.
Where a change of more than one quantum occurs, the peak obtained is called an overtone. As we shall see, in Raman scattering this occurs only in special circumstances. In most Raman spectra overtones are predicted as very weak or non-existent.
Further, vibrations can combine so that one quantum of one vibration and one of another vibration will give a new level. In the spectrum, peaks due to these combinations are called combination bands and like overtones appear only in certain circumstances. To make mat-

ters even more complicated, rotational levels, which are of lower energy than vibrational levels, also require to be added.

To describe the process of absorption when an electron is excited from one electronic state to another, a Morse curve for the ground and excited state is required with the excited state plotted above the ground state since it will be at higher energy. In Raman scattering all excited vibronic state have an influence on scattering efficiency. As a result, in principle, we require to raw Morse curves for all states of the molecule. However, the influence of each state is not specific and hence a simpler diagram as show in Figure 3.2 can be used in which all the many excited vibronic levels from the many excited electronics states are rapresented by a few lines.

Further, since Raman scattering is fast compared to the time for nuclear movement, there is no appreciable change in the nuclear separation during any scattering event and therefore no change along the x-axis. Thus, for a simple description of the process, energy change in the molecule are plotted as vertical lines and the states as horizontal lines with the other features of the Morse curve neglected.

In figure 3.2 it show the energy changes which occur when the exciting radiation interacts with the molecule to form a virtual state and the scattering which follows when the molecule relaxes. The scattered radiation is what we measure as Raman scattering and the energy difference between the excitation and scattering processes corresponds to the energy of vibrations of the molecule.

The shape of the Morse curve makes it difficult, but not impossible, to calculate the energy of vibronic levels and so simple theory uses the harmonic approximation. In this approach, the Morse curve shown is replaced by a parabola calculated for a diatomic molecule by considering it as two masses connected by a vibrating spring.

With this approach, Hooke's law (Equation 3.5) gives the relationship between frequency, the mass of the atoms involved in the vibration and the bond strength for a diatomic molecule:

$$\nu = \frac{1}{2\pi c}\sqrt{\frac{K}{\mu}} \tag{3.5}$$

where c is the velocity of light, K is the force costant of the bond between A and B and μ is the reduced mass of the atom A and B of masses M_A and M_B;

$$\mu = \frac{M_A M_B}{M_A + M_B} \tag{3.6}$$

Two other point should be noted. The harmonic approximation predicts that the overtones of a molecule are equally spaced but the reality is that the departure from harmonicity in a real system will mean that, particularly at higher energies, the energy separations between levels will decrease. For example, in Figure 3.3 which shows a Morse curve for one vibration, all the vibrational levels are shown as they actually are, with a decreased separation in energy the higher the vibrational quantum number. They would be shown equally spaced in the harmonic approximation. Further, the electron density along the vibration is of importance in working out the efficiency of the Raman process [33].

3.4 Polarization and Raman intensity

When radiation is emitted from a source, a number of photon are emitted and each photon consist of a oscillation dipole. Observed at 90° to the direction of propagation, the beam looks like a wave. Observed looking along the line between the observer and the light source, each photon will appear as a line, with the oscillating dipole in that line.

The lasers that are normally used for excitation in Raman scattering are usually at least partially polarized. Good Raman spectrometers also have an optical element, a polarizer, that can be put in the beam to ensure that the light is linearly polarized.

When linearly polarized light interacts with the molecule, the electron cloud is distorted by an amount that depends on the ability of the electrons to polarize (i.e. the polarizability, α). The light causing the effect is polarized in one plane, but the effect on the electron cloud is in all directions. This can be described as a dipole change in the molecule in each of the three Cartesian co-ordinates x, y and z. Thus, to describe the effect on molecular polarizability of an interaction with linearly polarized radiation, three dipoles require to be considered. The simple expression is that a dipole μ is created in the molecule by the field from the incident photon E.

$$\mu = \alpha E \tag{3.7}$$

To allow for the polarization angle of the linearly polarized light, the polarizability components of the molecule are usually labelled, an example of which is shown below:

$$\alpha_{xx}$$

The first subscript x refers to the direction of polarisability of the molecule, and the second x refers to the polarization of the incident light. Thus, $\mu_x = \alpha_{xx}E_x + \alpha_{xy}E_y + \alpha_{xz}E_z$. Similar expessions will exist for both μ_y and μ_z.

Thus, the polarizability of the molecule is a tensor:

$$\begin{bmatrix} \mu_x \\ \mu_y \\ \mu_z \end{bmatrix} = \begin{bmatrix} \alpha_{xx} & \alpha_{xy} & \alpha_{xz} \\ \alpha_{yx} & \alpha_{yy} & \alpha_{yx} \\ \alpha_{zx} & \alpha_{zy} & \alpha_{zz} \end{bmatrix} \begin{bmatrix} E_x \\ E_y \\ E_z \end{bmatrix} \tag{3.8}$$

There are specific advantages of this rather complex arrangement. In Raman scattering the incident and scattered beams are related. If radiation of a particular polarization is used to create the Raman scattering, the polarization of the scattered beam is related to but not necessarily the same as that of the incident beam. Thus, a Raman spectrometer has an optical elements, the polarizer, to control the polarization of the incident beam. It ensures that the radiation is plane polarized and determines the angle of the plane of the incident radiation.

A second element, the analyser, analyses the polarization of the scatterd beam. The analyser works by allowing the polarized light to pass through to the detector only in one plane. It's initially set to allow transmission of scattered radiation in the plane of the incident radiation

(called parallel scattering).
It's then set at 90° to this direction to allow any light in which the polarization direction has been changed by the molecule to pass through to reach the detector (called perpendicular scattering). This arrangiament is shown in Figure 3.4.

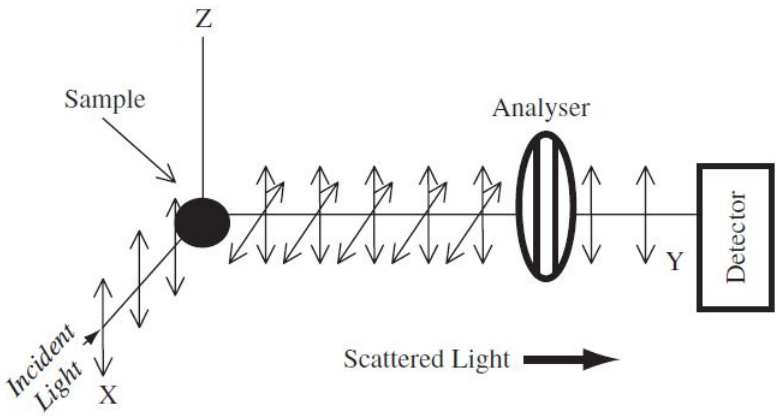

Figure 3.4: Arrangement to monitor polarization of Raman scattering. The arrows indicate the plane of the scattered light. The analysis is set to allow through only parallel scattering. If rotated 90° it will allow through only perpendicular scattering.

If a single crystal is used as a sample, all molecular axes are lined up within the unit cell in the same direction for each cell. The polarization direction of the incident radiation bears a relationship to the molecular axes. With an arrangement like this, it is possible to analyse each of the components of the tensor shown above.
Light is a dipole property, which means that the optical axes of a material are set at 90° to each other. In some higher symmetry space groups such as the tetragonal space group, the optical and crystal axes are at right angles and so they can be aligned to match the polarization direction of the incident beam. Under these circumstances, light polarized in the z direction, passing through the crystal along the *z-axis*, will pick out the component α_{zz}. In all likelihood there will be a molecular axis along the z-axis and so the information can be related to molecular properties.
However in most situations the analysis is more complex. Light which is not sent down an axis of the crystal will rotate within it and in many crystal space groups, the crystal axes are not at right angles and bear a complex relationship to the molecular axes. Thus this approach is very informative for a very limited number of samples.
Often, the samples we examine are either in the gas phase or in solution. In either case there is no ordering of the axes of the molecule to the polarization direction of the light but information can still be obtained from polarization mesasurements. What is measured in practice is the depolarization ratio where the intensity of a given peak is measured with the plane of polarization of the incident light parallel or perpendicular to the scattered light analysed.

For samples such as this, it is useful to express the average polarizability in terms of two separate quantities that are invariant to rotation, namely isotropic and anisotropic scattering. Isotropic scattering is measured with the analyser parallel to the plane of the incident radiation and anisotropic scattering with the analyser perpendicular to the plane. It is possible to solve the tensor and calculate the ratio of parallel to perpendicular scattering. This ratio is what is actually measured. It is called the depolarization ratio (ρ). Here we illustrate the salient equations but do not give details since this ratio is usually used qualitatively and is often talked about but seldom calculated.

$$\bar{\alpha} = \frac{1}{3}(\alpha_{xx} + \alpha_{yy} + \alpha_{zz}) \tag{3.9}$$

$$\gamma^2 = \frac{1}{2}[(\alpha_{xx} - \alpha_{yy})^2 + (\alpha_{yy} - \alpha_{zz})^2 + (\alpha_{zz} - \alpha_{xx})^2 + 6(\alpha_{xy}^2 + \alpha_{xz}^2 + \alpha_{yz}^2)] \tag{3.10}$$

$$\bar{\alpha}_{\parallel}^2 = \frac{1}{45}(45\bar{\alpha}^2 + 4\gamma^2) \tag{3.11}$$

$$\bar{\alpha}_{\perp}^2 = \frac{1}{15}\gamma^2 \tag{3.12}$$

The Equation 3.9 and 3.10 rapresented the isotropic and anisotropic part of the tensor, the Eq. 3.11 and 3.12 rapresented the effect on parallel and perpendicular polarization.
This gives a ratio between parallel and perpendicular scattering as:

$$\rho = \frac{\bar{\alpha}_{\perp}^2}{\bar{\alpha}_{\parallel}^2} = \frac{3\gamma^2}{45\bar{\alpha}^2 + 4\gamma^2} \tag{3.13}$$

For a molecule with appreciable symmetry in solution or in the gas phase, the depolarization ratio varies depending on the symmetry of the vibration. Symmetric vibrations have the lowest depolarization ratios. Thus measurement of parallel and perpendicular scattering using the analyser to obtain the depolarization ratio provides a check on assignments of the peaks. This check is not available with absorption spectroscopies such as infrared.
When radiation from the analyser is detected via a monochromator, the efficiency of the grating used to split up the light is dependent on the plane of polarization. This means the grating will transmit radiation to the detector more efficiently for either parallel or perpendicular polarization and consequently the apparent depolarization ratio will be wrong. The most conventional way to overcome this problem is to add an extra element, a scrambler, which scrambles the polarization of the light before it enters the monochromator so that the detector is equally efficient for all polarization directions of the incoming radiation.
It is interesting to now consider how these components of polarization, propagation and angular dependence of the incident and scattered radiation can be related to the intensity of the Raman radiation. This quantity also depends in a complex way on the polarizability of the molecule, the intensity of the source, the scattering cross section and many other parameters. The intensity of Raman scattering is defined by Eq. 3.14:

$$I = Kl\sigma^2\omega^2 \tag{3.14}$$

where K consists of constants such as the speed of light, l is the laser power, ω the frequency of the incident radiation and α the polarizability of the electrons in the molecule. Thus, two

of the parameters which are variable are under the control of the spectroscopist, who can set the laser power and the frequency of the incident light. The power and the frequency it depends on the laser used [34].
In our case, we don't care the Raman intensity becouse we use the relative intensity, so we dont't treat all the theory of the Raman intesity.

3.5 Number and symmetry of vibrations

With any molecule, the energy can be divided into translational energy, vibrational energy and rotational energy. Translational energy can be described in terms of three vectors 90° to each other and so has three degrees of freedom.
Rotational energy for most molecules can also be described in terms of three degrees of freedom. However, for a linear molecule there are only two rotations. The molecule can either rotate around the axis or about it. Thus, molecules are said to have three translational degrees of freedom and three rotational degrees of freedom with the exception of linear molecules, which have two degrees of rotational freedom. All other degrees of freedom will be vibrational degrees of freedom and each is equivalent to one vibration. Therefore, the number of vibrations to be expected from a molecule with N atoms is $3N - 6$ for all molecules except linear systems where it is $3N - 5$.
From this it is possible to work out the number of vibrations which occur. However, it must be noted that this does not make the vibrations either Raman or infrared active and in general we would not expect to observe all vibrations in either spectroscopy.

3.6 Symmetry elements and point groups

Any molecule can be classified by its symmetry elements (i.e. axes and planes). It is then possible to assign the molecule to a group called a point group which has these same elements. This can then be used to predict which bands are infrared and which are Raman active. To do this it is necessary to work out the symmetry elements in the molecule. The main symmetry elements we need to recognize are the following:

- E – The identity element. This takes the molecule back into the same position it started from;
- Cn – An axis of symmetry in which the molecule is rotated about a molecular axis. n Defines how often the molecule requires to be rotated to arrive back at the starting point.
- σ_h – A plane of symmetry in which the plane is perpendicular to the principle axis of the molecule.
- σ_v – A plane of symmetry in which the plane is parallel to the principle axis of the molecule.

- i – A centre of inversion in which every point inverted through the centre arrives at an identical point on the other side.
- S_n - An axis which combines a rotation and an inversion.

These symmetry elements define a particular type of molecule. All molecules with the same set of symmetry elements are said to belong to the same point group. To assign a molecule to its point group, the symmetry elements are first recognized and then analysed according to a set of rules. Usually symmetry elements are not analysed to assign a molecule to a particularly high symmetry point group such as the cubic point group, the octahedral point group and the tetrahedral point group. These can usually be recognized immediately. The questions we ask to make an assignment are set out in order below:

1. What's the principle axis of the molecule?
2. Is there a set of n C_2 axes at right angles to it? If the answer is no, carry on with the questions below. If the answer is yes, go to question 6.
3. Is there a plane perpendicular to the principle axis? If so, this is a σ_h plane. A molecule which has a C_n principle axis and a σ_h plane can be assigned to the point group C_{nh}.
4. If there is no σ_h plane, are there planes of simmetry parallel to the principle axis? There should be as many planes of symmetry as the n value. If this is the case, the point group is assigned as C_{nv}.
5. If there are no planes, the point group is assigned as C_n.
6. If the molecule has a principle axis and a set of n C_2 axes at right angles to it, is there a plane of symmetry perpendicular to the principle axis (i.e. a σ_h plane)? If this is the case, this molecule belongs to the D_{nh} point group.
7. If there is no σ_h plane of symmetry, is a set of n σ_v planes parallel to the principle axis? If the answer to this question is yes, then the point group is D_{nd}.
8. If there are no planes of symmetry, the molecule will belong to the D_n point group.

Or you can use the following scheme:

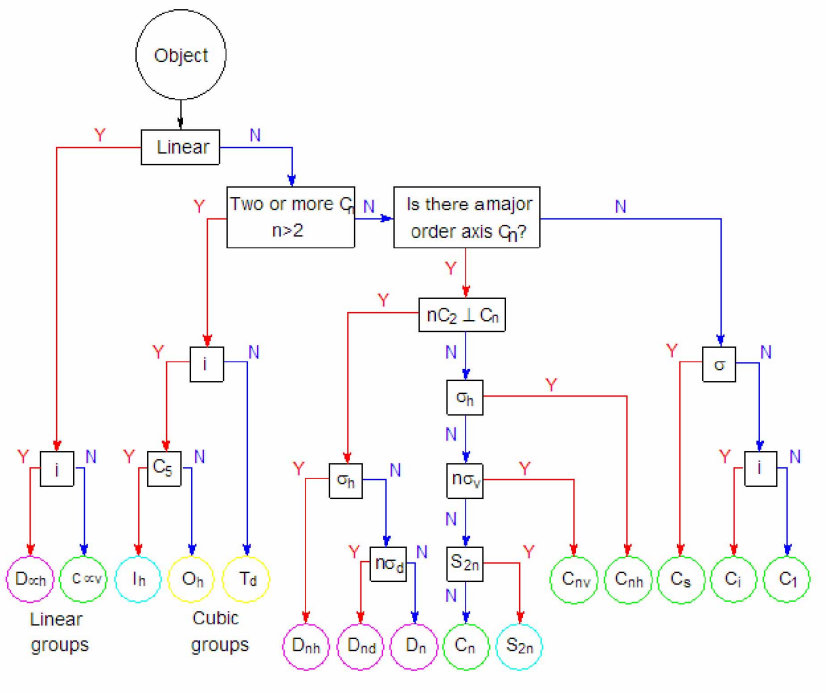

Figure 3.5: Point group scheme.

3.7 The mutual exclusion rule

One crucial result which arises from this analysis is that irrespective of other symmetry considerations, for a centrosymmetric molecule, only vibrations which are g in character can be Raman active and only vibrations which are u in character can be infrared active. This is because irrespective of the exact irreducible representation, the g and u labels can be multiplied out and the final product must contain the totally symmetric representation and hence g. The rules are $gxg = g, uxu = g$ and $gxu = u$. Since the Raman operators are g in character and the ground state is g, the excited state must be g if the vibration is to be allowed. In contrast, the infrared operator is u in character and so the excited state must be u if the vibration is to be allowed. Thus, in a molecule with a centre of symmetry, vibrations which are Raman active will not be infrared active, and vibrations which are infrared active will not be Raman active. This analysis leads to a rule known as the mutual exclusion rule, which states that any vibration in a molecule containing a centre of symmetry can be either Raman or infrared active, but not both. In molecules without a centre of symmetry, there is no such specific rule. Nonetheless, in general, symmetric vibrations are more intense in Raman scattering and asymmetric vibrations in infrared scattering.

3.8 Confocal mode

When the laser spot is focused onto a solid or liquid sample, the property of the beam, such the penetration depth and its shape, strictly depends by the refractive index and the absorption characteristics of the material. Hence, the Raman scattering will occur within this so-called probe volume and detected with different intensity along the beam length and across the focal plane. Therefore, the spectrum measured from a point on the surface of the sample will carry with it the information, sometimes undesired, from the crystallographic planes below the surface.

However, the T64000 Raman spectrometer is equipped with a set of cross-slit, which allow the modulation of the Raman probe and hence work in confocal mode, thus excluding those information from the region out-of-focus. The confocal microscopy, patented by Minsky in 1957 [35], is a well-known technique commonly employed in the Raman spectroscopy and in other imaging microscopy. As depicted in Figure 3.7(a) Through two filtering pinhole, one placed on the laser beam path (enhancing the Gaussian shape of the probe) and the other one located in the exit focal plane of the microscope (improving both lateral and axial space resolution), it is possible to exclude the light originating from the out-of-focus planes.

The signal from the surface is brought to a focus at the aperture and passes without significant attenuation. On the other hand, out-of-focus light from below the surface is brought to a focus before the aperture and is thereby cut off. Nevertheless, for a quantitative deconvolution of the Raman spectra within a set of given focal planes, this approach needs to be coupled with a theoretical characterization of the laser probe geometry when it interacts with the sample. This means that a detailed knowledge of the "probe response function" (PRF) is required, which must be experimentally determined in each single case.

The PRF, depending on the geometry and the physical properties of the sample, is composed of two main terms, as showed in Figure 3.7 (b) and (c): the in-plane probe response $G_{ip}(x, y, x_0, y_0)$ and the in-depth probe response $G_{ip}(z, z_0)$. The first term takes into account the lateral resolution and can be calculated acquiring the Raman intensity as a function of the in plane displacement (x_0) of the probe, while the second one gives the in-depth resolution and can be calculated by defocusing the probe along the axis normal to the sample surface (z_0).

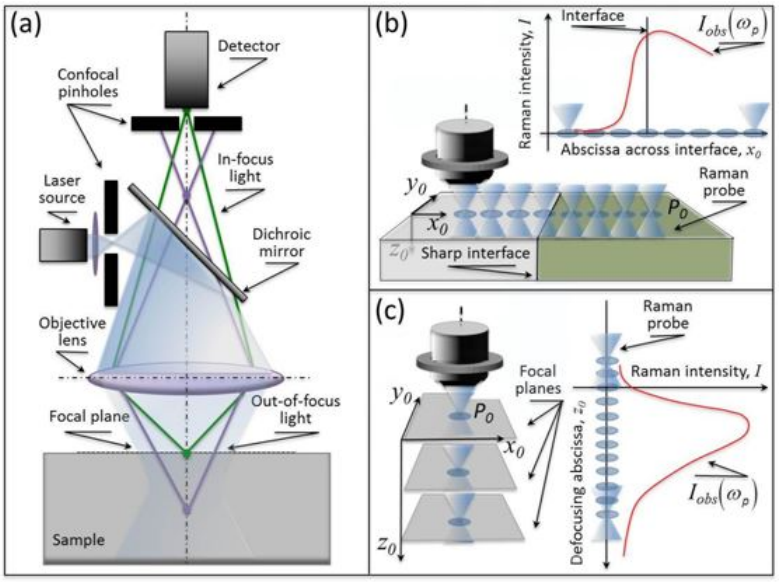

Figure 3.6: (a) Schematic draft of the confocal configuration for Raman assessments. Methods of PRF calibrations for quantitatively representing in-plane and in-depth probe structure and morphology are shown in (b) and (c), respectively.

Thus, the observed intensity of the Raman spectrum depends on the geometrical distribution (the PRF) of the scattered light around the irradiation point. Following the reference [36] [37], when the laser is focused on a given position $P_0(x_0, y_0, z_0)$, the PRF, that is a convolution of the in-plane and in-depth probe response, weighting the intensity of the light scattered from a point P(x,y,z), can be expressed as:

$$G(x, y, z, x_0, y_0, z_0) \propto G_{ip}(x, y, x_0, y_0) \times G_{ip}(z, z_0) =$$

$$= exp\left[-2\frac{(x - x_0)^2 + (y - y_0)^2}{R^2}\right] \frac{p^2}{(z - z_0)^2 + p^2} exp(-2\alpha z) \tag{3.15}$$

Where R is the radius of the laser beam in the focal plane, p is the probe response parameter, (which for an unfocused beam tends to infinity), and α is the absorption coefficient of the material at the incident wavelength.

3.9 Instrumentation

As briefly discussed in the introduction of this chapter, a micro Raman apparatus able to record Raman spectra generally consists of five main components: a source of monochromatic light to induce the Raman scattering; a microscope device to focus incident and collect the Raman light; a spectrograph, that split the collected light in a spectrum of frequencies, a detector, which transduce the light in an electrical signal; a post-acquisition software, which serve as visual interface able to display the spectrum of frequency. The instrumentation, which is able to correctly visualize and display a noise-free Raman scattering spectrum, consists also in several fundamental component. Among them is worthy to note the notch filter that can cut-off the elastic Rayleigh scattering of the laser and the optical polarizer,

which enable the collection of the polarized Raman light. All the spectroscopic experimental results reported in this thesis were carried out at room temperature, in a backscatter configuration, using a micro-Raman spectrometer (T-64000, Horiba/Jobin-Yvon., Kyoto, Japan). An overall view of the instrument is shown in Figure 3.8.

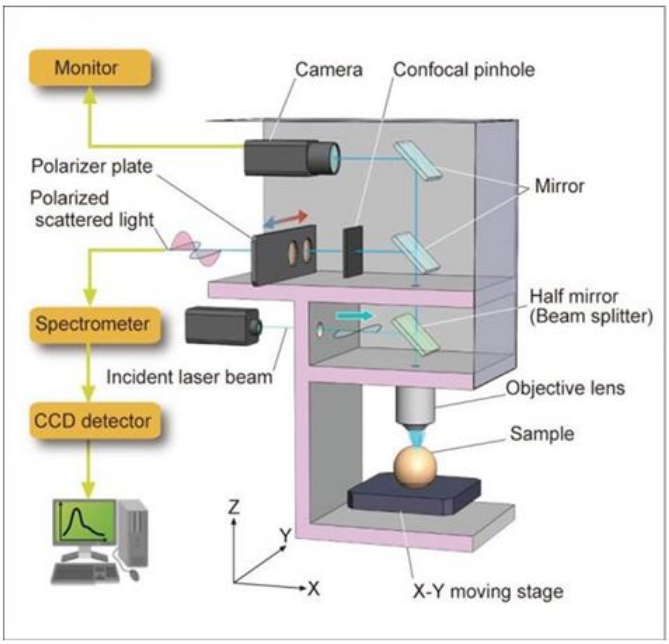

Figure 3.7: Schematic draft of the T-64000 Raman spectrophotometer.

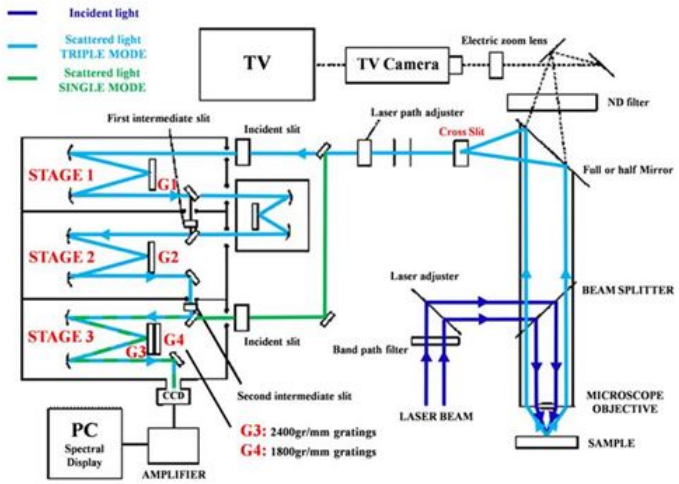

Figure 3.8: Operative scheme of the T-64000 spectrophotometer.

The T64000 spectrometers can basically work in two different modes: a single configuration in which only one monochromator, the spectrograph, is employed (stage 3 in Figure 3.9) and a triple configuration (stage 1 and 2 in Figure 3.9) before the spectrograph. The detector used to acquire the spectrum is a multichannel 1024 x 256 pixels CCD camera device (CCD-3500V, Horiba Ltd., Kyoto, Japan) mounted in the plane of the exit image.

The CCD is liquid-nitrogen cooled down to 140K.

During the experiments, one laser line were used as light excitation source: a continuous wave (CW) water-cooled 488 nm Ar-ion laser (Stabelite 2017, Spectra Physics, Mountain View, CA, USA) operating with a power of 200 mW. The laser beam is focused on the sample by means of an optical microscope, which has three different objective long focus lenses: a 100x objective lens with NA=0.9, a 50x objective lens with NA=0.X and a 20x objective lens with NA=0.9. The 100x objective lens, the most used during the experiments, allows obtaining a spot size of about 1 μm. Since the light is collected in backscattering configuration, the scattered light must be separated from the incident beam using a beam splitter.

Chapter 4

Results and discussion

4.1 *In vitro* analysis of ZTA with different metal stains

Predictions of the *in vivo* stability of the tetragonal polymorph in ZTA femoral heads are typically based on *in vitro* simulations in a hydrothermally activated environment. As reported in detailed studies [38] [39], the hydrothermal environment affects the stoichiometric state of tetragonal zirconia dispersoids and greatly accelerates the phenomenon of polymorphic transformation in ZTA. However, retrieval studies have suggested that the *in vivo* destabilization of tetragonal zirconia is likely a complex combination of different effects, rather than a single-effect driven phenomenon [40]. The long-term hydrothermal exposure cannot thus be considered as the only trigger for phase transformation, not even under normal service conditions and especially in the case of short-term retrievals [40] [41].
Moreover, our paper [42] demonstrated a large fluctuation in the initial monoclinic fraction for ZTA femoral head components, as-received from the maker, as a function of manufacturing year and, presumably, of raw material lots and manufacturing furnaces [41].
The theory of hydrothermally activated surface aging of ZTA materials, at its present stage of development, includes the effect of the initial monoclinic fraction, but simply as an additive factor to an otherwise independent isochronal or isothermal monoclinic fractional growth. The main aim of this chapter is to incorporate into a more comprehensive theoretical frame the two main causes of discrepancies between the amounts of monoclinic polymorphic transformation expected during *in vitro* aging in hydrothermal environment and those actually occurring during *in vivo* service. From the one hand, we located in the starting monoclinic phase fraction a fundamental parameter for correctly assessing the implant aging performance. Such parameter turns out to be key in distinguishing about the manufacturing quality of ZTA joint components as received from the maker.
On the other hand, the metal transfer phenomenon is considered here as another key phenomenon in solving *in-vitro/in-vivo* discrepancies. Described as the result of impingement against the metallic acetabular shell following subluxation/dislocation, smeared metal stains

on ceramic femoral heads are typical evidence for joint malfunctioning [43] [44] [45]. Accordingly, we systematically incorporated the metal transfer phenomenon in the experimental protocol of hydrothermal aging of ZTA. This practice represented the most straightforward way to assess whether or not metal stains could contribute to the destabilization of the tetragonal zirconia phase in ZTA bioceramics. Experimental data including the effects of initial monoclinic fraction and different types of metal stain represent the phenomenological frame on which we built up an implemented theoretical formulation. Predictions according to such implemented theory appear to narrow the gap between *in vitro* and *in vivo* data.

We selected commercial ZTA femoral heads manufactured in 2009 which possessed 21% of initial monoclinic fraction. The initial monoclinic fraction depends from on manufactured years, production company and as a result of the materials and their percentages [40]. We analyzed a ZTA with the following composition: 80 vol.% Al_2O_3, 17 vol.% Yttria stabilized ZrO_2 (Yttria content in zirconia grains is 1.3 mol.%), 3 vol.% strontium aluminate platelets. The samples were cut into several pieces and each was subjected to *in vitro* accelerated aging treatments that were performed for up to 100h in a conventional water-vapour autoclave operating at 98∼132°C under adiabatic pressure. Some of the examined ZTA femoral head components were eventually stained with different types of metal (i.e., Ti, CoCr, and Fe) in order to simulate the *in vivo* formation of metal contamination upon impingement against the metallic acetabular shell in consequence of subluxation/dislocation.

The spectrum integration time was typically 5 s, averaging the recorded spectra over three successive measurements. A confocal configuration of the Raman probe was adopted throughout all the experiments, using a 100x objective lens in order to exclude photons scattered from out-of-focus regions of the probe. The ZTA samples were placed on an x-y axes motorized stage (lateral resolution of 0.1μm), which allowed the collection of Raman maps on the femoral head surface. Intensity and spectral positions of selected Raman bands were obtained upon fitting the raw collected spectra with mixed Gaussian/Lorentzian curves.

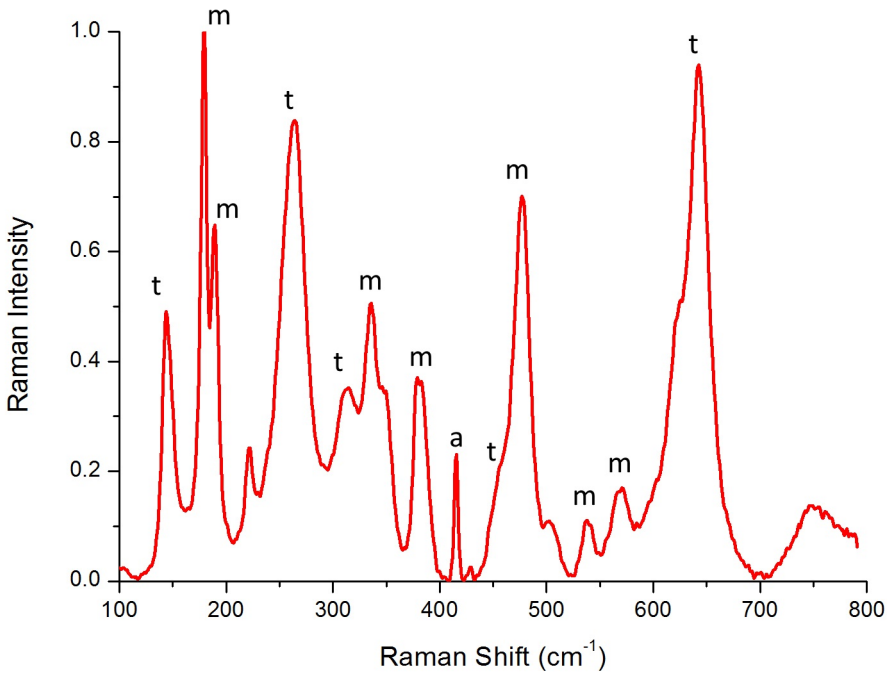

Figure 4.1: A typical Raman spectrum of ZTA.

Figure 4.1 shows a typical Raman spectrum of ZTA. The tetragonal (t) and the monoclinic (m) zirconia bands were assigned according to the literature [46] [47], and there is only one band detected at about 419 cm^{-1} in alumina.

There are several formulas to calculate the monoclinic volume fraction. In the work of Tabares et al. [48], they have compared different formulas to calculate the monoclinic volume fraction. In our case we used the Katagiri formula, which uses only the lower wavenumber parts of the Raman spectrum (cf. Figure 4.2). Tabares et al. found that the Katagiri formula is more precise than the widely applied method proposed by Clarke et al. [49], which was found to underestimate the fraction of the monoclinic phase.

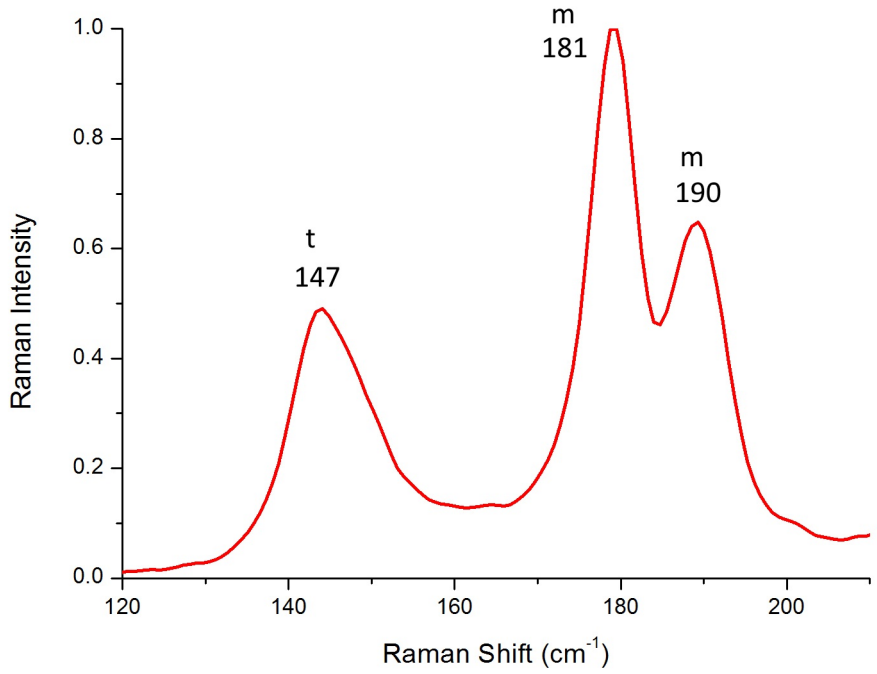

Figure 4.2: A typical Raman spectrum of the transformed region.

Figure 4.2 shows a typical Raman Spectrum of the transformed region. The overlapping bands peaking at 190 and 181 cm^{-1} are attributed to the monoclinic phase and the 147 cm^{-1} band is due to the tetragonal phase. The monoclinic volume fraction (Vm) can be expressed by the Katagiri equation that uses the peak intensity of the monoclinic and tetragonal Raman bands:

$$Vm = \frac{1/2(I_m^{181} + I_m^{190})}{kI_t^{147} + 1/2(I_m^{181} + I_m^{190})} \tag{4.1}$$

where k(=2.2) is a correcting factor for the difference of scattering cross section between the monoclinic and tetragonal Raman bands [50].

Figure 4.3 shows the experimental results of isothermal aging tests conducted at 121°C. The plot was given in a semi-logarithmic time scale for as-manufactured ZTA components, which showed different initial volume fractions, V_{0m}, of monoclinic phase.

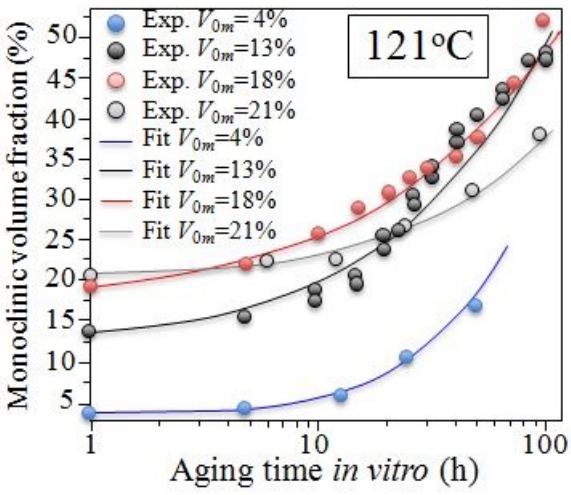

Figure 4.3: Experimental results of isothermal aging tests conducted at 121°C.

The plotted fractions correspond to fractions of the total amount of the zirconia phase in the ZTA composite (i.e.,∼17% in volume). Data are compared with those previously published [39] [51], which were also confirmed in this study. Rationalization of *in vitro* collected data of hydrothermally activated polymorphic transformation in zirconia-containing materials is usually attempted according to a modified the Mehl-Avrami-Johnson (MAJ) equation [52], as follows:

$$V_m = V_{0m} + (V_{max} - V_{0m})[1 - exp(-b^n t^n)] \tag{4.2}$$

where V_m is the monoclinic phase content for a given test duration t, V_{0m} is the initial monoclinic phase content prior to the test, V_{max} is an apparent upper bound of the monoclinic phase, n the time (or Avrami) exponent, and b is a factor that describes the temperature dependence of the aging effect. This latter factor is considered to follow a hydrothermally activated (Arrhenius) dependence, according to the following equation:

$$b = b_0 * exp\left(-\frac{Q}{RT}\right) \tag{4.3}$$

where b_0 is a material constant, Q is the activation energy for phase transformation during environmental aging, R the universal gas constant, and T the absolute temperature.
Isochronal characterizations at fixed temperatures could then be followed as a means of obtaining the parameter Q from the slope of an Arrhenius plot according to Eq. 4.3. Such plots are shown in Fig. 4.4 for samples with different initial contents of monoclinic fraction, V_{0m}, and the obtained values are used for fitting the isothermal data in Fig. 4.3.

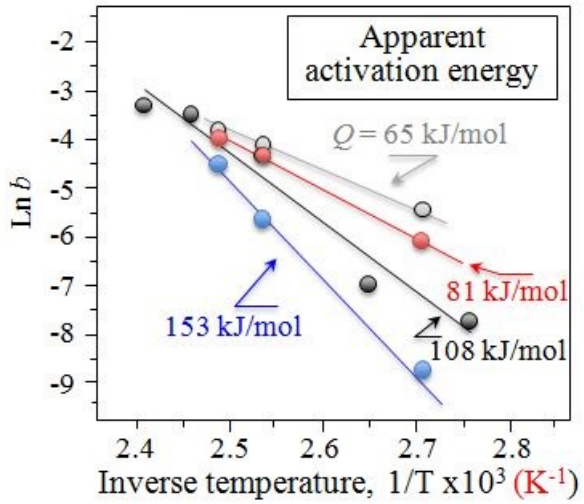

Figure 4.4: Value of Q from the slope of Arrhenius plot.

The most striking output of this procedure is that we actually find different activation energy values, Q, for samples with different V_{0m}. Note that one could use the value of V_{max} as a dummy parameter to fit different experimental curves with acceptable precision within limited intervals of time.

However, there is no physical reason why the parameter V_{max} should differ if exactly the same ZTA material is tested. In fitting data in Fig. 4.3, we have used V_{max}=100%, namely the total amount of zirconia phase available in the ZTA material. The obtained (apparent) Q values could be plotted as a function of V_{0m} according to a monotonic curve (Fig. 4.5).

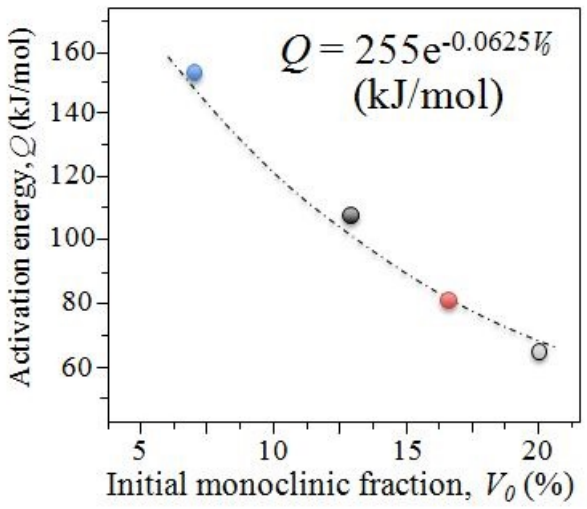

Figure 4.5: Value of Q to vary from V_0.

They indeed showed large fluctuations, the ZTA sample with the highest amount of monoclinic phase in its as-received state (V_{0m}=21%) displaying a value, Q=65 kJ/mol, twice as smaller as that of the ZTA sample with the lowest V_{0m} (i.e., $\sim$ 7%) in the investigated series. The different behaviors could also be attributed to stoichiometric differences among

different lots of raw materials (e.g., including fluctuations in the stabilizing Y_2O_3 content). However, we shall assume here, in first approximation, that all the tested ZTA samples were manufactured in the same way, and check whether or not the MAJ algorithm could explicitly contain a dependence on V_{0m}. If this attempt proves successful, the transformation process could be considered as isokinetic for ZTA ceramics, and the MAJ-like fitting procedure could become valid beyond its merely phenomenological correspondence with *in vitro* experimental data.

Additional experimental plots are shown in Figs. 4.6(a)∼(d) for a selected ZTA femoral head with V_{0m}=21%, whose dome area was cut into a number of different samples and tested under isothermal conditions (at 98, 121, and 132°C) without (a) and with artifi-cially staining by CoCr (b), Fe (c), and Ti (d). Data in (a) complete the trend already observed in Fig. 4.3 and serve as a reference for comparing with the stained samples. It should be noted that the artificial staining procedure turned out to be a quite easy task to conduct in the laboratory, with the metallic rods "writing" on the ZTA samples as chalk on a blackboard.

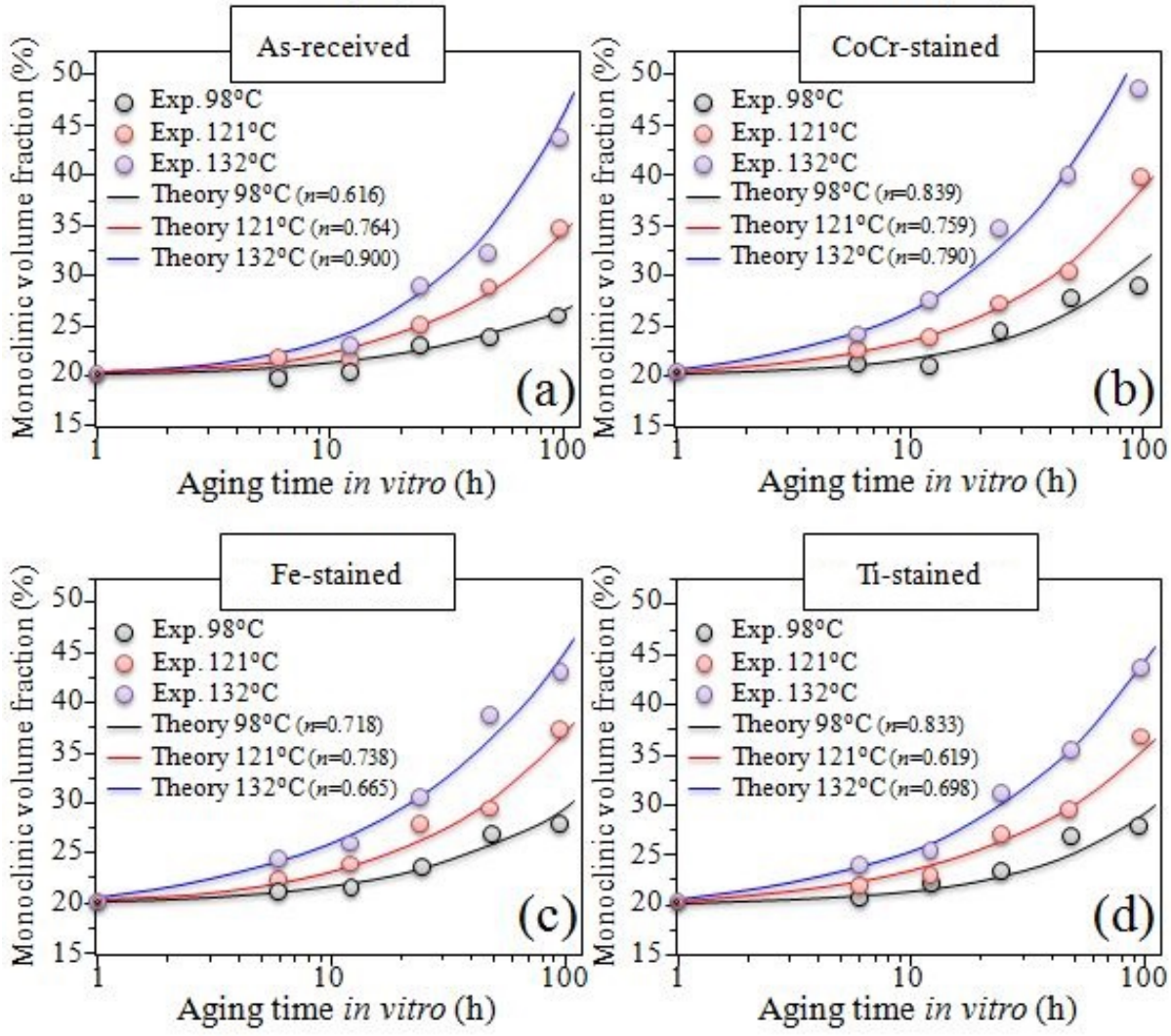

Figure 4.6: Experimental isothermal plots at V_{0m}=21% for 98, 121, and 132°C.

Data in Fig. 4.6 show that all the stained ZTA samples, concurrently aged in hydrothermal environment, experienced a conspicuously quicker polymorphic transformation as compared to the unstained sample, despite the fact that all samples were made of exactly the same material.

Among the metal-stained samples, those contaminated with CoCr were the quickest to transform, reaching Vm values of ∼50% and 40% after 100 h at 132 and 121°C, respectively. These laboratory results thus provide straightforward and systematic evidence to explain the unexpectedly high amounts of monoclinic phase in femoral head retrievals contaminated by metal stains upon malfunctioning *in vivo*.

In a kinetic model of phase transformation, the overall effective activation energy, Q, should incorporate the activation energies for nucleation, Q_N, and for growth, Q_G, as follows:

$$Q = \frac{\frac{d}{m}Q_G + (n - \frac{d}{m})Q_N}{n} \tag{4.4}$$

where m is a growth mode parameter (equal to 1 and 2 for interface-controlled and volume-diffusion-controlled growth, respectively), d=1, 2, or 3 is the dimensionality of the growth and n is a numerical parameter equal to d/m for site saturation and $d/m+1$ for continuous nucleation [53] [54].

The relationship between the effective (i.e., overall) activation energy, Q, and its separate components for nucleation and growth, Q_N and Q_G, which has been analytically validated by Liu et.al.[53], considers two activation energy components (as constant values), intrinsic to the physical processes involved. However, the effective activation energy, Q, depends on time and/or temperature through the growth exponent, n. Accordingly, Q could be constant during the transformation only under extreme (and limiting) kinetic conditions. In other words, not only a genuine variation of Q should be expected with progressing transformation, but also different values should be retrieved for different initial amounts of nuclei (i.e., for different V_{0m} values).

According to the above considerations, for isochronal cycles Eq. 4.2 should be rewritten, as follows:

$$V_m = 1 - (1 - V_{0m})exp\left[-b_0^n t^n exp\left(-\frac{nQ}{RT}\right) * \left(\frac{RT^2}{\Phi}\right)^n\right] \tag{4.5}$$

with $\Phi = \dfrac{dT}{dt}$ being a constant heating rate, n and Q are function of temperature, and the latter is given by Eq. 4.4.

Note that, in Eq. 4.5, the term containing the heating rate disappeared in our experiments since they were conducted at a constant temperature and the effect on transformation of heating/cooling periods during the cycle was negligible. In the case of isothermal cycles, the governing equation becomes:

$$V_m = 1 - (1 - V_{0m})exp\left[-b_0^n exp\left(-\frac{nQ}{RT}\right) * t^n\right] \tag{4.6}$$

where both n and Q are function of time. Theoretical curves and the related n values retrieved by best fitting of the experimental data to Eq. 4.6 were used to fit the experimental data in Figs. 4.3 and 4.6(a)∼(d) for samples differing in V_{0m} and with different metal stains,

respectively.

The retrieved n values are given in inset to each plot. As a general trend, the n value increased with increasing testing temperature, with initially higher volume fractions of monoclinic phase, and in the presence of metal stain (with values for CoCr being the highest at any investigated temperature).

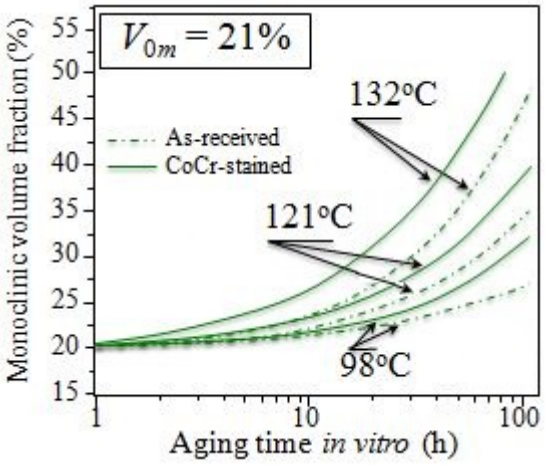

Figure 4.7: Curves of no-stain and CoCr-stained.

Figure 4.7 shows a comparison between isothermal curves recorded for no-stain and CoCr-stained samples with V_{0m}=21%. The comparison clearly shows the detrimental effect of metal stain on the stability of the ZTA bearing surface. Moreover, an activation energy value could yet be retrieved upon rearranging Eq. 4.5, as follows:

$$ln\tilde{V} = ln\left[ln\left(\frac{1-V_{0m}}{1-V_m}\right)\right] = n(lnb_0 + lnt) - \frac{nQ}{RT} \tag{4.7}$$

Accordingly, the slope of a plot of $ln\tilde{V}$ vs. $\frac{1}{T}$ is thus $\frac{nQ}{R}$, while the slope of a plot of $ln\tilde{V}$ vs. lnt simply becomes n.

Note that the formalism adopted in Eq. 4.7 yet foresees the existence of an intrinsic (i.e., constant) activation energy, Q, for the transformation phenomenon, but allows variations of the apparent activation energy value, $Q_{app} = nQ$, since n is a function of temperature.

Such plots are summarized in Fig. 4.8 for the as-received sample in comparison with the full series of stained samples with a common V_{0m}=21%. The comparison shows that the slopes of plots corresponding to stained samples located lowered values of activation energy. Moreover, the values always lied higher than those collected on the as-received sample for any type of metal stain. The representative plot for CoCr showed the highest shift as compared to the non-stained sample.

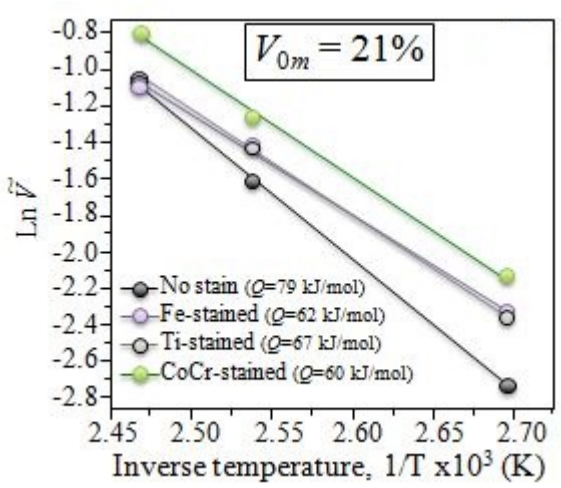

Figure 4.8: Value of Q from the slope of Arrhenius plot of the as-received sample and stained samples.

This means that also a sensitive variation of the quantity, $n(lnb_0 + lnt)$, occurred for a common (constant) time of hydrothermal exposure. One step forward was then taken in describing the concurrent effect of V_{0m} and metal stain on the evolution of the transformed surface. Experiments were repeated on stained samples with different V_{0m}. The results of these latter experiments are plotted in Fig. 4.9. The plot describes the gap between the temperature-dependent parameter, $b = b_0 exp\left(-\frac{Q}{RT}\right)$ in presence and in absence of stain (i.e., b_s and b_{ns}, respectively) as a function of V_{0m}.

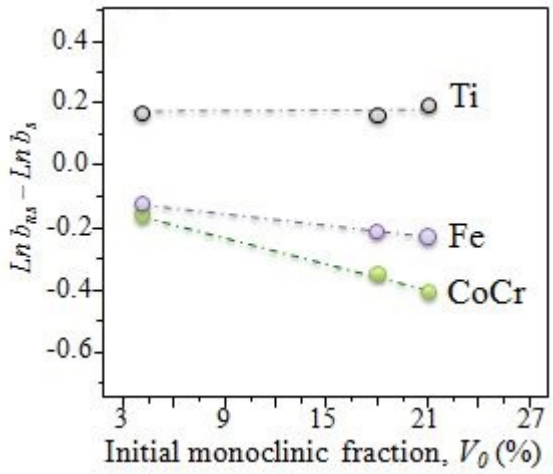

Figure 4.9: Effect of V_{0m} and metal stain on the evolution of the transformed surface.

As seen, as far as CoCr and Fe were concerned, the influence of stain reduced when the starting fraction of monoclinic phase decreased. However, this was not the case of Ti for which the detrimental effect on transformation remained substantially independent of V_{0m}. The data in Fig. 4.9 indeed confirmed that the influence of metal contamination is a function of the initial density of transformed nuclei on the sample surface. Let's briefly summarize the physical meaning of the above findings according to the structure of Eqs.

4.4∼4.7, as follows:

- The apparent increase in the value, $Q_{app} = nQ$, for polymorphic transformation (cf. Fig. 4.3), which accompanies an increase in V_{0m}, is due to a variation in the n value upon isothermal experiments. A closer look to Eq. 4.4 suggests that the origin of the dependence $n(T)$ should be searched for in a change in dimensionality, d, if the growth mode parameter is unchanged. More specifically, it is the structure of n and its dependence on T that leads to the observed difference.

- Besides the above argument, one cannot rule out the possibility that the observed fluctuations in monoclinic fraction for the ZTA femoral heads only (or also) arise from fluctuation in the Y_2O_3 content contained in the raw material lots, the lower the content the higher V_{0m} and the more meta-stable the bearing surface during service.

- The presence of metal stain at the surface alters the b_0 and the Q_{app} parameters significantly. This effect should thus be discussed in terms of chemical triggers during thermal activation.

Finally, one could notice that the n values depended on the presence and type of stain but their temperature dependence fluctuated within a relatively narrow interval for each type of sample. Accordingly, we assumed an average n value as obtained from the temperature interval 98°∼132°C (cf. n values in inset to Fig. 4.6). With the knowledge of n, the Q values could then be obtained from the slopes of the plots $ln\tilde{V}$ vs. $\frac{1}{T}$ (cf. insets to Fig. 4.8). Using the experimentally determined Q values and Eq. 4.6, the hydrothermal aging effect under *in vivo* conditions (37°C) can be obtained from accelerated hydrothermal aging tests. In this latter calculation, the b_0 values at 37°C could be obtained from the extrapolation of Arrhenius plots of lnb_0 vs. $\frac{1}{T}$ for each different materials (i.e., at 37°C, $b_0 = 0.0278x10^{-5}, 4.469x10^{-5}, 8.548x10^{-5}$, and $2.511x10^{-5}$ for no-stain, CoCr, Ti, and Fe, respectively).

4.2 Retrieval study of ZTA femoral heads

Femoral heads made from ZTA ceramics are considered to be the most advanced bioceramic currently available for total hip arthroplasty (THA). ZTA is an improvement over prior generations of medical ceramics because of its higher strength and toughness. Its superior mechanical properties result from the polymorphic transformation of its zirconia phase under the local tensile stress field generated at the tip of a propagating crack [38].

However, unintended transformation can also spontaneously occur by exposure of the ceramic to biologic or hydrothermal environments, resulting in the annihilation of any toughening effect [55]. Recognizing this undesirable phenomenon, ZTA ceramics have been intensely studied over the years to lessen their proneness to polymorphic transformation [56]. However, positive *in vivo* confirmation of enhanced material stability is yet lacking. In fact, even short-term retrievals quite often reveal high amounts of transformation when compared to predictive *in vitro* models [40].

The stability of zirconia in severe hydrothermal environment is a function of chemical composition and grain size [38] [57]. For a given ZTA microstructure, the long-term aging *in vivo* can be predicted under the assumption that both formation and successive growth of monoclinic nuclei on the material surface are thermally activated. Under such hypothesis, subjecting the zirconia polycrystal to systematic variations of temperature for increasing periods of time leads to determine a value of thermal activation energy in a controlled hydrothermal environment. The output of such an experiment is represented by curves of monoclinic phase fraction as a function of temperature and time of environmental exposure. With the experimental knowledge of a value of activation energy, temperature extrapolations can be made to predict the increase of monoclinic fractions *in vivo* as a function of time.

The present phenomenological investigation was undertaken to screen deeper into the phenomenon of polymorphic transformation. As a first item, we attempted to improve the statistics on the as-manufactured implants released to the market with checking about whether or not through the years the ZTA manufacturer succeeded in keeping uniform the quality of femoral heads with respect to the surface amount of monoclinic contents. A further goal of this investigation consisted in comparing *in vivo* data of monoclinic fractions on the bearing surface with predictions formulated according to activation energy arguments and hip-simulator tests. Finally, *in vitro* spectroscopic experiments were focused on determining if fluctuations in pristine monoclinic fraction from the manufacturing process and/or metal ions incorporated during *in vivo* service in the joint space (i.e., CoCr, Ti, and Fe) could be responsible for triggering accelerated phase changes in the ZTA material.

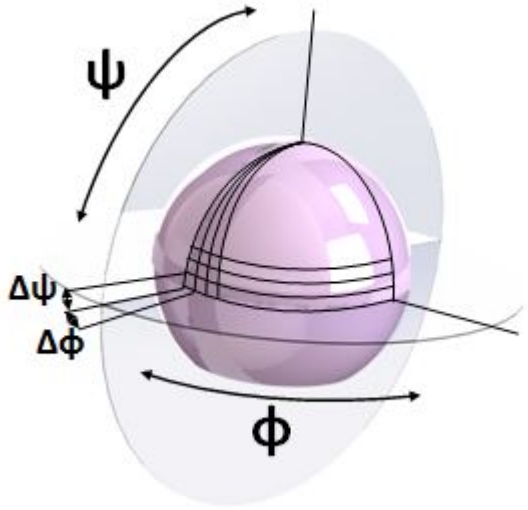

Figure 4.10: Femoral head with the different sections.

Figure 4.10 shows a reproduction of the femoral head. In it are represented the axes, horizontal Φ and vertical Ψ, used to create a grid on the sphere. In sections of spheres obtained, we collected the Raman maps to study the entire surface and identify the wear areas of the prosthesis.

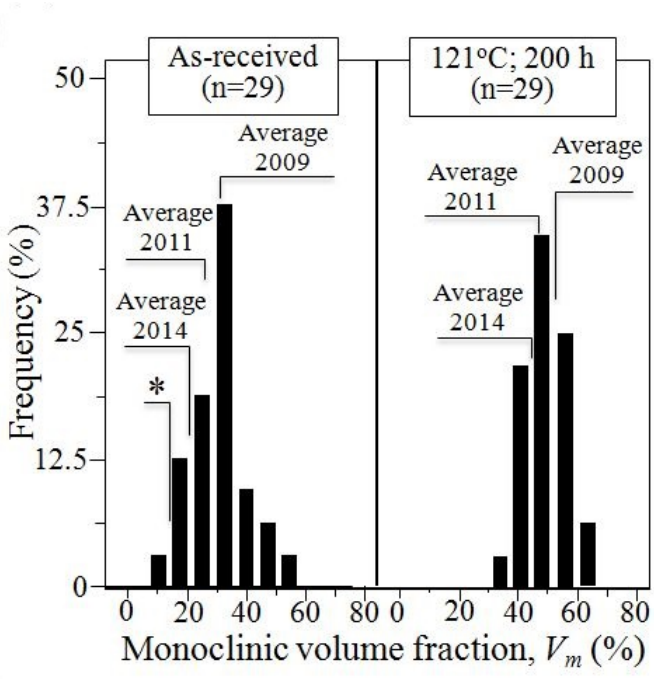

Figure 4.11: Statistical data collected on 29 ZTA femoral heads.

We conducted a retrieval study on 29 ZTA femoral heads [39] [58].

Figure 4.11 shows statistical data collected on 29 ZTA femoral heads as received from the maker and manufactured in the decade 2005-2015. There are two types of prosthesis: Cereamic-on-Polyethylene (CoP) and Ceramic-on-Ceramic (CoC). The plot reports about the fraction of heads that experienced a given average fraction of monoclinic phase on their surface after manufacturing (left plot) and after an autoclave cycle at 121°C in hydrothermal environment (right plot). The left plot is relatively broad and locates femoral heads released to the market with an average surface fraction of monoclinic polymorph fluctuating between 10 and 55% for the constituent zirconia phase. In inset, average values located for individual years are also plotted, which show a higher average fraction for heads manufactured in 2009. While average data grouped according to manufacturing years actually show an improvement through the years in limiting the amount of monoclinic phase at the surface of the released components, the general data trend also shows a wide variety of surface condition for the marketed heads. The effect of autoclaving the heads in hydrothermal environment is that of shifting the content of monoclinic polymorph toward higher fractions (i.e., in the interval 30∼65%), while narrowing the width of the statistical distribution and the differences among sets of components from specific manufacturing years.

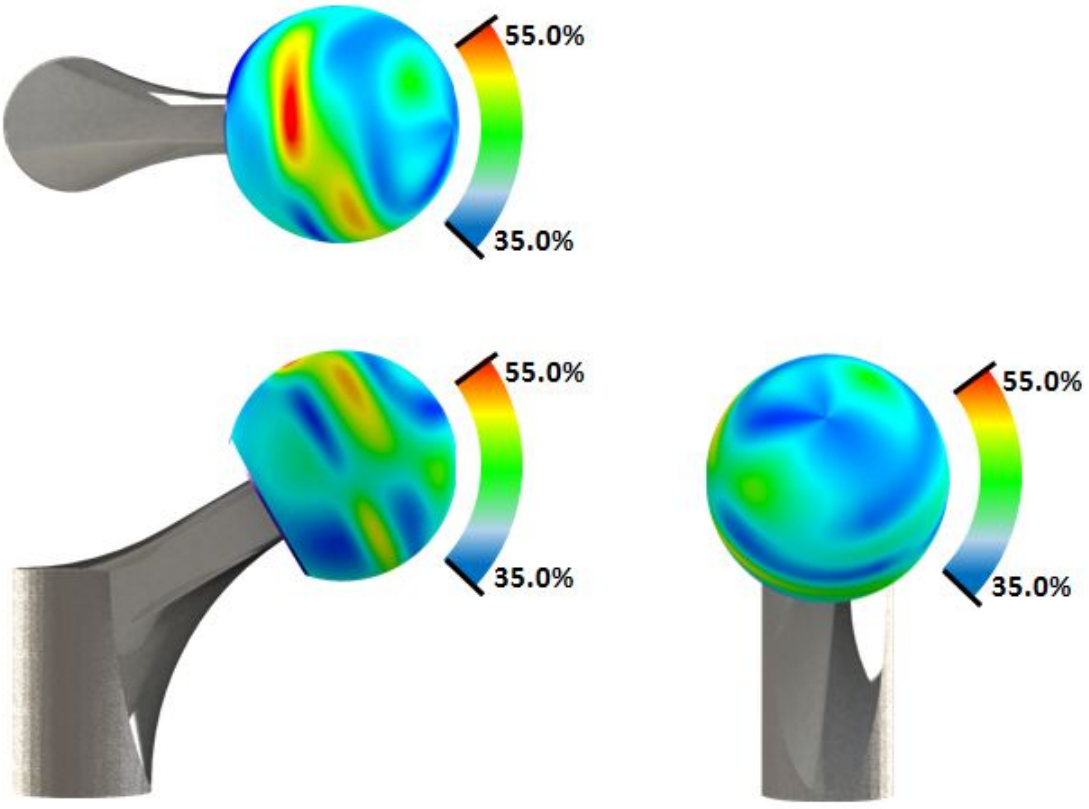

Figure 4.12: Monoclinic volume fraction of entire surface.

An example of Raman maps of the monoclinic volume fraction, V_m, on the entire surface of the retrieval is shown in Figure 4.12. To make these images, we have made small maps

on the whole surface of the sphere and then approached to create the image above. From this, it was possible to identify the Main Wear Zone (MWZ) and Non Wear Zone (NWZ), which are the most and the least transformed area respectively.

This is due to the fact that the MWZ is the work area of the prosthesis and therefore more subject to wear and residual stress. Conversely, the NWZ is the area of the prosthesis where it is not practiced no stress and then only turns the effect of the temperature and the biological environment. It may be noted also that on the surface are not well defined the MWZ and NWZ area, because on some retrieval are present, on the surface, some metal smears. These areas are called Stripe Wear Zone (SWZ). These metal contaminations are due to a contact between the ceramic part and the metal of the implant (stem or acetabular cup).

Not all metallic stain have the same form, in fact Fredette et al. [59] have cataloged different kinds of metal stain from different retrievals. In our case we are not cataloged smears depending on the shape and type, but only analyzed the amount of transformed phase present on the surface.

After having identified the MWZ and NWZ area, it was possible to orient the femoral head in its working position.

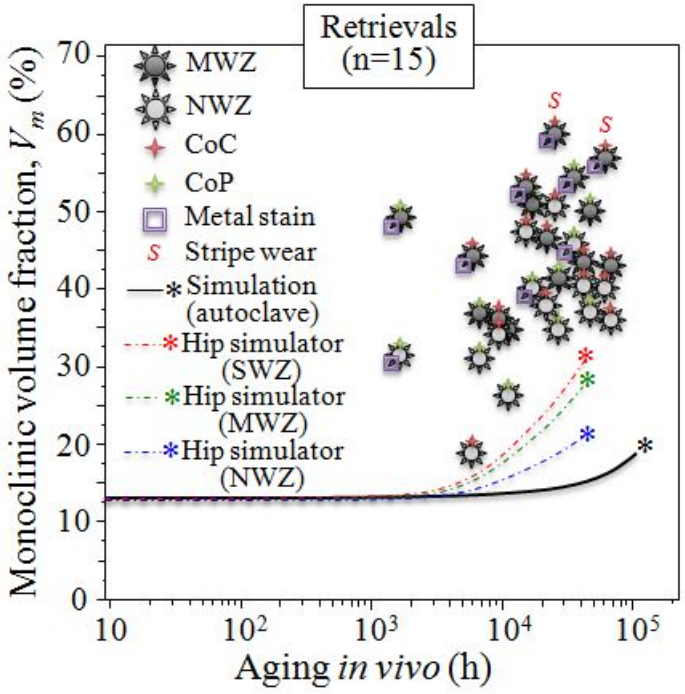

Figure 4.13: Monoclinic fractions averaged in MWZ and NWZ on 15 CoP and CoC femoral head retrievals plotted against the number of years elapsed in vivo.

In Fig. 4.13, monoclinic fractions averaged in MWZ and NWZ on 15 short- and medium-term femoral head retrievals are plotted against the number of years elapsed in vivo before revision surgery. Besides distinguishing between MWZ and NWZ, different symbols are added to locate whether the implant was of the ceramic-on-polyethylene (CoP) or ceramic-on-ceramic (CoC) type, and whether or not metal stain and/or a SWZ appeared on the

head surface after explantation. Comparisons were carried on with ZTA samples tested in a hip simulator equipped to perform CoC self-mating experiments with microseparation displacements. The contents of monoclinic polymorph relative to NWZ, MWZ, and SWZ were plotted in the same graph of the retrievals under the assumption that 1 ml cycles in the hip simulator corresponded to 1 y *in vivo*. Moreover, a reference curve was also drawn as an extrapolation to body temperature of hydrothermal data collected upon high-temperature (accelerated) *in vitro* tests in autoclave [39].
In this case they are not used, the simulated data of the first part, but only those made previously using the equation 4.2 of the MAJ model, without considering the effect of V_{0m} and the effect of activation energies for nucleation, Q_N, and for growth, Q_G.
The outputs of the composite plot in Fig. 4.13 could be summarized, as follow:

- Independent of location on the retrieval surface, all the retrievals showed a content of monoclinic polymorph significantly higher than those obtained in hip simulator or predicted by extrapolating in vitro aging data in autoclave.

- MWZs generally experienced higher amounts of transformed monoclinic fraction than NWZs independent of the type of implants. Although the SWZ in the examined ZTA heads was never clearly visible under the optical microscope, the highest fractions of monoclinic phase were reached in zones corresponding to possible impingements against the metallic cup as revealed by the presence of metal stain.

- In general, the presence of metal stain enhanced the rate of polymorphic transformation, with significantly higher amounts of monoclinic phase being found in correspondence of stained surfaces.

Following analysis of the entire surface to identify the different areas of interest, it was desired to see the progress of the transformation in depth. In this case we collected the Raman spectra in the same condition (confocal mode), but we change the focus, as explained in section 3.1.8, to increase the probe analyzed and also analyze just below the surface zone. To do this, first we found the index of refraction of the ZTA (corresponding to 1.785) so as to be able to know precisely the depth to which the measurement is made. We analyzed different depths (0, 5, 10, 20, 50, 100 μm) in the MWZ, the NWZ and finally the SWZ.

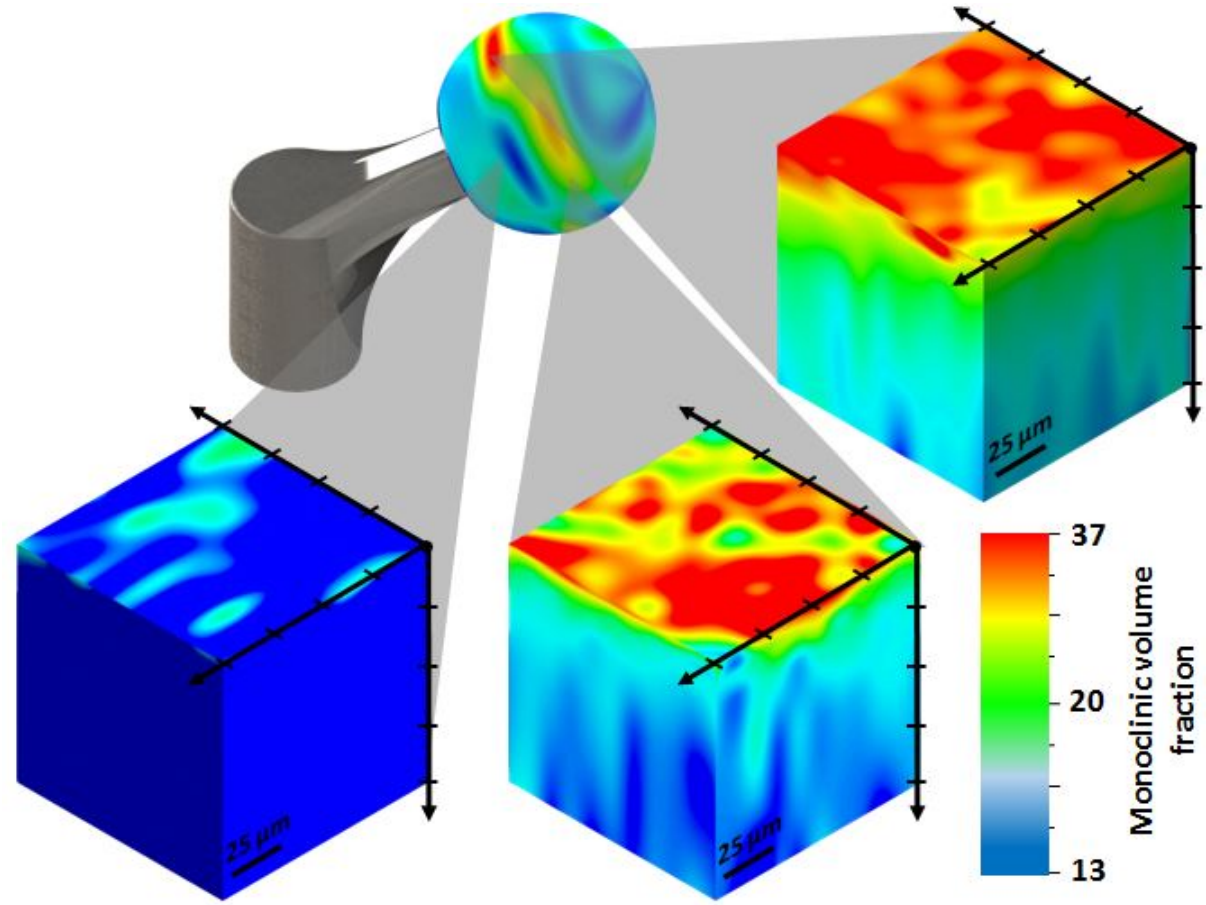

Figure 4.14: In-depth maps of the different areas.

As a result, we can observe the profiles of V_m at different depths in different areas, as shown in Figure 4.14. In this retrieval it can be observed that there is a big difference between the MWZ area and NWZ. We can also see how the transformation is mainly concentrated on the surface. As the depth increases in MWZ, the transformation becomes less, until almost varies in the bulk. In the area of SWZ, we can see the transformation is almost similar to the MWZ area. In the case of the NWZ, only the very surface shows a slight phase transformation.

We noticed that in most of the retrieval analyzed with depth maps, that the transformation of the zirconia occurs mainly in the first 20μm of the surface and below this depth, it becomes nearly negligible. The same thing, a little less obvious, takes place in the area of the SWZ, where the influence of the metallic smear leads to a greater transformation of NWZ.

Chapter 5

Conclusions

Crystallographic destabilization of the ZTA bearing surfaces was experimentally substantiated as the consequence of an ensemble of different phenomena, which includes not only hydrothermal activation but also the initial monoclinic volume fraction of the components and the presence of metal contaminations at the transformation sites. These additional factors were taken into account in an implemented theoretical frame, which allows judging about material stability of ZTA implants operating under real conditions in a way more realistic than pre-existing models. One main output of this investigation was the observation of a change in the apparent activation energy, Q, with the initial volume fraction of monoclinic phase in the as-manufactured component. This dependence can be included in the predictive algorithm and should not be considered as an experimental artifact or as a consequence of changes of transformation mechanism. Moreover, a chemical effect related to the presence of metal ions could be clearly located by *in vitro* experiments. This is indeed an extrinsic factor, which plays a preponderant role in accelerating ZTA surface destabilization also in absence of elevated surface stresses (i.e., in hard-on-soft implants) and even if, after dislocation reduction, the kinematics of the joint articulation takes place correctly. It is hoped that this work could provide the manufacturer of ZTA joint components with a rejuvenated stimulus to release to the market a product with lower V_{0m} and better uniformity.

In the second part, where the retrieval of several years of production and with different V_{om} were analyzed, we observed the difference in monoclinic volume fraction between the MWZ and the NWZ. These data have been reported in Fig. 4.13 where we see how the data obtained from retrieval,deviate from the simulated data.
The results of the calculation of the first part, the hydrothermal aging effect under *in vivo* conditions (37°C), are plotted in Fig. 5.1 for samples with and without stains in the case of V_{0m}=21%. The retrieval data described in the second part, and the prediction from Chevalier et al. [39] (V_{0m}=13%), are also included for comparison.

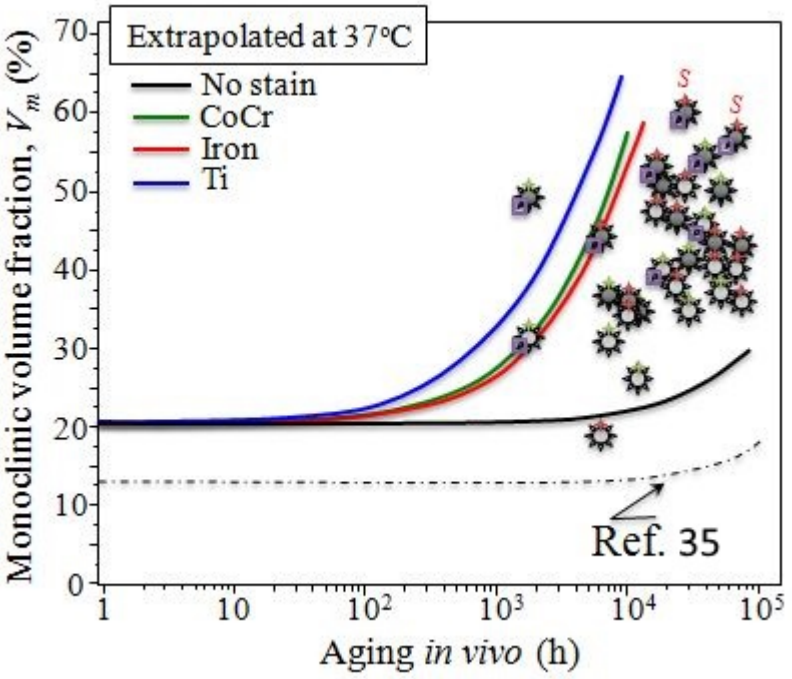

Figure 5.1: Extrapolations to body temperature of monoclinic contents for samples with and without stains in the case of V_{0m}=21% and also included the retrieval data.

By doing so, the mismatch between *in vivo* and *in vitro* data appears greatly reduced. According to the newly proposed algorithm, which takes into consideration the role of V_{0m}, the dependence *b(T)*, and the influence of metal stain, more realistic estimations appear to be possible for the expected lifetime of a ZTA artificial joint according to *in vitro* accelerated tests. So we can think that, as mentioned earlier, the metal contamination of the surface combined with the biological environment, increases the T-M transformation of the ZTA.

Bibliography

[1] Hip Joint - Anatomy Pictures and Information.

[2] Angela Bellato. *Artroprotesi totale dell'anca: passato, presente e futuro.*

[3] Robin Del Pozo, Jose, Patel. Infection Associated with Prosthetic Joints. *New England Journal of Medicine*, 361(8):787–794, 2009.

[4] J Vander Sloten, Luc Labey, R Van Audekercke, and G Van der Perre. Materials selection and design for orthopaedic implants with improved long-term performance. *Biomaterials*, 19:1455–1459, 1998.

[5] W J Maloney, M Jasty, A Rosenberg, and W H Harris. Bone lysis in well-fixed cemented femoral components. *J Bone Joint Surg Br*, 72(6):966–970, 1990.

[6] Rock M 1933, German patent Drp N°583589.

[7] Sandhaus S. 1965 British Patent N°1083769.

[8] C Piconi, G Maccauro, F Muratori, and E Brach Del Prever. Alumina and zirconia ceramics in joint replacements. *Journal of applied biomaterials & biomechanics : JABB*, 1:19–32, 2003.

[9] C. Piconi and G. Maccauro. Zirconia as a ceramic biomaterial. *Biomaterials*, 20(1):1–25, 1999.

[10] Robert Heimann and Hans Lehmann. Bioceramics – A Historical Perspective. *Bioceramic Coatings forMedical Implants: Trends and Techniques*, pages 1–10, 2015.

[11] J D Helmer and T D Driskell. Research on bioceramics. Symp. on Use of Ceramics as Surgical Implants, 1969.

[12] P Christel, A Meunier, J M Dorlot, J M Crolet, J Witvoet, L Sedel, and P Boutin. Biomechanical compatibility and design of ceramic implants for orthopedic surgery. *Annals of the New York Academy of Sciences*, 523:234–256, 1988.

[13] Jérôme Chevalier and Laurent Gremillard. The Tetragonal-Monoclinic Transformation in Zirconia: Lessons Learned and Future Trends. 1920:1901–1920, 2009.

[14] Marcella Elpers, Denis Nam, Susie Boydston-White, Michael P Ast, Timothy M Wright, and Douglas E Padgett. Zirconia phase transformation, metal transfer, and surface

roughness in retrieved ceramic composite femoral heads in total hip arthroplasty. *The Journal of arthroplasty*, 29(11):2219–23, 2014.

[15] O Ruff and F Ebert. Contributions on the ceramics of highly fireproof material I The forms of zirconium dioxide, 1929.

[16] Ronald C Garvie and Patrick S Nicholson. Structure and Thermomechanical Properties of Partially Stabilized Zirconia in the CaO-ZrO2 System, 1972.

[17] R. C. Garvie, R. H. Hannink, and R. T. Pascoe. Ceramic steel? *Nature*, 258(5537):703–704, 1975.

[18] G. S. a. M. Theunissen, J. S. Bouma, a. J. a. Winnubst, and a. J. Burggraaf. Mechanical properties of ultra-gine grained zirconia ceramics. *Journal of materials science*, 27:4429–4438, 1992.

[19] James S Reed and Anne Marie Lejus. Affect of grinding and polishing on near-surface phase transformations in zirconia. *Materials Research Bulletin*, 12(10):949–954, 1977.

[20] T. Sato and M. Shimada. Control of the tetragonal-to-monoclinic phase transformation of yttria partially stabilized zirconia in hot water. *Journal of Materials Science*, 20:3988–3992, 1985.

[21] C. Piconi, W. Burger, H. G. Richter, a. Cittadini, G. Maccauro, V. Covacci, N. Bruzzese, G. a. Ricci, and E. Marmo. Y-TZP ceramics for artificial joint replacements. *Biomaterials*, 19(16):1489–1494, 1998.

[22] J J Swab. Low temperature degradation of Y-TZP materials. *Journal of Materials Science*, 26(24):6706–6714, 1991.

[23] Zirconia as a sliding material: histologic, laboratory, and clinical data.

[24] Jérôme Chevalier, Laurent Gremillard, and Sylvain Deville. Low-Temperature Degradation of Zirconia and Implications for Biomedical Implants. *Annual Review of Materials Research*, 37(1):1–32, 2007.

[25] Hassan El Attaoui. Influence du renforcement sur le comportement en fatigue statique et cyclique des céramiques monolithiques de type Alumine et Zircone. *Sciences-New York*, 2003.

[26] D.J. Kim, H.J. Jung, J.W. Jang, and H.L. Lee. Fracture Toughness, Ionic Conductivity, and Low-Temperature Phase Stability of Tetragonal Zirconia Codoped with Yttria and Niobium Oxide. *Journal of the American Ceramic Society*, 81:2309–2314, 1998.

[27] Felicia M. Pitek and Carlos G. Levi. Opportunities for TBCs in the ZrO2-YO1.5-TaO2.5 system. *Surface and Coatings Technology*, 201(12):6044–6050, 2007.

[28] Jens Schneider, Sabine Begand, Ralf Kriegel, Christian Kaps, Wilfried Glien, and Thomas Oberbach. Low-temperature aging behavior of alumina-toughened zirconia. *Journal of the American Ceramic Society*, 91(11):3613–3618, 2008.

[29] Dan Gutknecht, Jérôme Chevalier, Vincent Garnier, and Gilbert Fantozzi. Key role of processing to avoid low temperature ageing in alumina zirconia composites for orthopaedic application. *Journal of the European Ceramic Society*, 27(2-3):1547–1552, 2007.

[30] Dong-woo Shin, K. K. Orr, and Helmut Schubert. Microstructure-Mechanical Property Relationships in Hot Isostatically Pressed Alumina and Zirconia-Toughened Alumina. *Journal of the American Ceramic Society*, 73(5):1181–1188, 1990.

[31] C He, Y S Wang, J. S. Wallace, and S M Hsu. Effect of microstructure on the wear transition of zirconia-toughened alumina. *Wear*, 162-164(PART A):314–321, 1993.

[32] W. Burger and H.G. Richter. High Strength and Toughness Alumina Matrix Composites by Transformation Toughening and 'In Situ' Platelet Reinforcement (ZPTA) - The New Generation of Bioceramics. *Key Engineering Materials*, 192-195:545–548, 2001.

[33] Derek a Long. *The Raman Effect*, volume 8. 2002.

[34] E. Smith, G. Dent, and J. Wiley. *Modern Raman spectroscopy: a practical approach*. 2005.

[35] M Minsky. Memoirs on Inventing the Confocal Scanning Microscope. *Scanning*, 10(1 988):128–138, 1988.

[36] A Atkinson and S C Jain. Spatially Resolved Stress Analysis Using Raman Spectroscopy. *Journal of Raman Spectroscopy*, 30(10):885–891, 1999.

[37] Keshu Wan, Wenliang Zhu, and Giuseppe Pezzotti. Determination of in-depth probe response function using spectral perturbation methods. *Journal of Applied Physics*, 98(11), 2005.

[38] Jérôme Chevalier. What future for zirconia as a biomaterial?, 2006.

[39] Jérôme Chevalier, Sylvie Grandjean, Meinhard Kuntz, and Giuseppe Pezzotti. On the kinetics and impact of tetragonal to monoclinic transformation in an alumina/zirconia composite for arthroplasty applications. *Biomaterials*, 30(29):5279–5282, 2009.

[40] S Affatato, E Modena, A Toni, and P Taddei. Retrieval analysis of three generations of Biolox femoral heads: Spectroscopic and SEM characterisation. *Journal of the Mechanical Behavior of Biomedical Materials*, 13:118–128, 2012.

[41] M Boffelli, A Doimo, E Marin, L Puppulin, W Zhu, N Sugano, I.C. Clarke, and G Pezzotti. Chemically driven tetragonal-to-monoclinic polymorphic transformation in retrieved ZTA femoral heads from dual mobility hip implants. *Journal of the Mechanical Behavior of Biomedical Materials*, 56:195–204, 2016.

[42] Giuseppe Pezzotti, Wenliang Zhu, Matteo Zanocco, Elia Marin, Bryan J Mcentire, Jérôme Chevalier, and B Sonny Bal. Reconciling in vivo and in vitro kinetics of polymorphic transformation in zirconia-toughened alumina for hip joints :I. Phenomenology. 2016.

[43] Young-Hoo Kim, Allan Ritchie, and Cath Hardaker. Surface roughness of ceramic femoral heads after in vivo transfer of metal: correlation to polyethylene wear. *The Journal of bone and joint surgery. American volume*, 87(3):577–82, 2005.

[44] Ivan M Tomek, John H Currier, Michael B Mayor, and Douglas W Van Citters. Case Report Metal Transfer on a Ceramic Head With a Single Rim Contact. *Journal of Arthroplasty*, 27(2):324.e1–324.e4, 2012.

[45] B. Sonny Bal, Mohamed N. Rahaman, Thomas Aleto, F. Scott Miller, Francesco Traina, and Aldo Toni. The Significance of Metal Staining on Alumina Femoral Heads in Total Hip Arthroplasty. *Journal of Arthroplasty*, 22(1):14–19, 2007.

[46] C. M. Phillippi and K. S. Mazdiyasni. Infrared and Raman Spectra of Zirconia Polymorphs. *Journal of the American Ceramic Society*, 54(5):254–258, 1971.

[47] M Ishigame and T Sakurai. Temperature-dependence of raman-spectra of ZrO2. *Journal of the American Ceramic Society*, 60:367–369, 1977.

[48] José A. Muñoz Tabares and Marc J Anglada. Quantitative analysis of monoclinic phase in 3Y-TZP by raman spectroscopy. *Journal of the American Ceramic Society*, 93(6):1790–1795, 2010.

[49] D R Clarke and F Adar. Measurement of the crystallographically transformed zone produced by fracture in ceramics containing tetragonal zirconia. *Journal of the American Ceramic Society*, 65(6):284–288, 1982.

[50] Gen Katagiri. Direct determination by a Raman microprobe of the transformation zone size in Y2O3 containing tetragonal ZrO2 polycrystals, 1988.

[51] Giuseppe Pezzotti, Kiyotaka Yamada, Seiji Sakakura, and Rocco Paolo Pitto. Raman spectroscopic analysis of advanced ceramic composite for hip prosthesis. *Journal of the American Ceramic Society*, 91:1199–1206, 2008.

[52] Jerome Chevalier, Bernard Cales, and Jean Michel Drouin. Low-Temperature Aging of Y-TZP Ceramics. 82(8):2150–2154, 1999.

[53] F. Liu, F. Sommer, and E. J. Mittemeijer. An analytical model for isothermal and isochronal transformation kinetics. *Journal of Materials Science*, 39(5):1621–1634, 2004.

[54] A. T W Kempen, F. Sommer, and E. J. Mittemeijer. The isothermal and isochronal kinetics of the crystallisation of bulk amorphous Pd40Cu30P20Ni10. *Acta Materialia*, 50(6):1319–1329, 2002.

[55] Giuseppe Pezzotti, Kiyotaka Yamada, Alessandro Alan Porporati, Meinhard Kuntz, and Kengo Yamamoto. Fracture toughness analysis of advanced ceramic composite for hip prosthesis. *Journal of the American Ceramic Society*, 92(8):1817–1822, 2009.

[56] Giuseppe Pezzotti. *Advanced Materials for Joint Implants*. 2013.

[57] Steven M. Kurtz, Sevi Kocagoz, Christina Arnholt, Roland Huet, Masaru Ueno, and William L. Walter. Advances in zirconia toughened alumina biomaterials for total joint replacement. *Journal of the Mechanical Behavior of Biomedical Materials*, 31:107–116, 2014.

[58] Giuseppe Pezzotti, Leonardo Puppulin, Marco Boffelli, Nobuhiko Sugano, Bryan J Mcentire, and B Sonny Bal. Metal Ions Contribute to the Material Instability of Zirconia Toughened Alumina. *Proceedings of the Annual Meeting of the Orthopaedic Research Society*, (c):Poster #1100, 2016.

[59] Eliza K. Fredette, Daniel W. MacDonald, Richard J. Underwood, Antonia F. Chen, Michael A. Mont, Gwo Chin Lee, Gregg R. Klein, Clare M. Rimnac, and Steven M. Kurtz. Does metal transfer differ on retrieved ceramic and CoCr femoral heads? *BioMed Research International*, 2015(February 2016), 2015.

Acknowledgements

I would like to thank the professor G. Pezzotti and the professor P. Riello for the opportunity to do this thesis at the KIT (Kyoto Institute of Technology).
A big thanks to Dr. W. Zhu for the help in all thesis and for the development of formulas used.
Also thanks to Dr. E. Marin and Dr. A. Rondinella for support in the second part, the help in the creation of beautiful images and support and friendship during the period done in Japan.
Last but not less important thanks to my family for the moral and financial support and thanks to Debora for having supported also in difficult times.